Available online at www.sciencedirect.com
ScienceDirect
Journal of Computational Physics 225 (2007) 568–590
JOURNAL OF COMPUTATIONAL PHYSICS
www.elsevier.com/locate/jcp

Electromagnetic gyrokinetic PIC simulation with an adjustable control variates method

R. Hatzky [a,*], A. Könies [b], A. Mishchenko [b]

[a] *Rechenzentrum der Max-Planck-Gesellschaft und des Max-Planck-Instituts für Plasmaphysik, EURATOM-Association, D-85748 Garching, Germany*
[b] *Max-Planck-Institut für Plasmaphysik, Teilinstitut Greifswald, EURATOM-Association, D-17491 Greifswald, Germany*

Received 20 January 2006; received in revised form 22 November 2006; accepted 18 December 2006
Available online 10 January 2007

Abstract

In the last decade, it became clear that electromagnetic (gyro)kinetic particle-in-cell (PIC) simulations are very demanding in respect to numerical methods and the number of markers used. The Monte Carlo discretization of the gyrokinetic equations leads to a severe signal-to-noise problem: the statistical representation of the physically irrelevant but numerically dominant adiabatic current causing a high statistical noise level. The corresponding inaccuracy problem is very pronounced at high plasma β and/or small perpendicular wave numbers $k_\perp$.

We derive several numerical schemes to overcome the problem using an adjustable control variates method which adapts to the dominant adiabatic part of the gyro-center distribution function. We have found that the inaccuracy problem is also present in the quasi-neutrality equation as a consequence of the $p_\parallel$-formulation [T.S. Hahm, W.W. Lee, A. Brizard, Nonlinear gyrokinetic theory for finite-beta plasmas, Phys. Fluids 31 (1988) 1940]. For slab simulations in the magneto-hydrodynamic (MHD) limit $k_\perp \to 0$, the number of markers can be reduced by more than four orders of magnitude compared to a conventional δf scheme.

The derived schemes represent first steps on a road to fully adaptive control variates method which can significantly reduce the inherent statistical noise of PIC codes.

MSC: 65M25; 77C10

PACS: 52.65.Rr; 52.30.Gz

Keywords: Gyrokinetic simulation; δf method; Control variates method; Electromagnetic

* Corresponding author. Tel.: +49 (0)89 3299 1707; fax: +49 (0)89 3299 1301.
E-mail address: roman.hatzky@rzg.mpg.de (R. Hatzky).

0021-9991/$ - see front matter
doi:10.1016/j.jcp.2006.12.019

1. Introduction

The δf method [1,2] is widely used for electrostatic particle-in-cell (PIC) simulations to discretize the gyro-center distribution function f_s of a species s. Its basic idea is the ansatz $f_s = f_{0s} + \delta f_s$ where the distribution function f_s is split into a time-independent background f_{0s} and a time-dependent perturbation δf_s. As long as the perturbed part δf_s remains small in comparison to the background part f_{0s} which is often chosen to be a Maxwellian, the δf method reduces the statistical noise. However, the conventional δf method as a noise reduction technique is an independent reinvention by the plasma physics community of a variance reduction method which can be traced back [3] to the standard Monte Carlo method called control variates method.

In principle, it is also possible to use the δf method for electromagnetic gyrokinetic PIC simulations [4], but the time step can be quite restrictive and the required number of markers can be so large that PIC simulations become impractical. Hence, in the past decade, many attempts have been made to improve electromagnetic PIC algorithms in two respects: the relaxation of the time step criterion and the reduction of statistical noise. A key part of these efforts was a modification of the δf ansatz known as the split-weight scheme.

The original split-weight scheme for electrostatic simulations [5] expanded the δf_e ansatz for electrons by their adiabatic response $ef_{0e}\phi/(k_B T_e)$ to the electrostatic potential $\phi(t)$. Its benefit is primarily the relaxation of the time step criterion, although there is some reduction in noise. The finite-β extension of the split-weight scheme is given in Ref. [6]. In this reference, with the focus on noise reduction, the adiabatic response $ef_{0e}\tilde{\psi}_{\mathrm{eff}}/(k_B T_e)$ of the electrons is extended to the effective potential $\tilde{\psi}_{\mathrm{eff}}(t) = \phi + \int \partial A_\parallel/(c\partial t)\,\mathrm{d}x_\parallel$.

The original split-weight scheme was generalized [7] to overcome both the constraint on the time step and the inaccuracy problem at high beta, $\beta \approx 1\%$. It uses the so-called $p_\parallel$-formulation [8] of the gyrokinetic Vlasov-Maxwell system (an alternative $v_\parallel$-formulation suffers from the numerical instability associated with the free streaming of the particles, see Ref. [9] for details). The inaccuracy problem, also called the cancellation problem (see e.g. Ref. [4]), results from the fact that the physically relevant nonadiabatic part of the electron distribution function is overwhelmed by the adiabatic response to the magnetic potential $A_\parallel$. It is a severe signal-to-noise problem especially at high beta and/or small perpendicular wave numbers $k_\perp$ where the relevant signal is so small that it is usually swamped by the statistical noise.

An enhanced control variates method [10] has been presented to solve the inaccuracy problem and not the constraint on the time step due to the fast parallel electron motion. The focus of this paper is to generalize this method. In contrast to the split-weight scheme, a modification of the δf_e ansatz is not necessary. Instead, on top of the δf_e ansatz, a further adjustable control variate is used to extract the dominant adiabatic part of the gyro-center distribution function from the statistical marker representation and to transfer it into an analytic representation. As consequence, the statistical noise level of the PIC method is significantly reduced. This is done for both the charge-assignment in the quasi-neutrality equation and the current assignment in Ampère's law. It is important to note that the inaccuracy problem is also present in the quasi-neutrality equation as a consequence of the $p_\parallel$-formulation and has to be handled properly in both field equations.

Three direct and two iterative schemes are derived based on the adjustable control variates method. A rigorous derivation of the two iterative schemes includes the specification of the condition of convergence. All five schemes are benchmarked for a linear slab problem in the magnetohydrodynamic (MHD) limit $k_\perp \to 0$. The slab problem has the advantage that it fully expresses the inaccuracy problem and the corresponding solution for the dispersion relation is known analytically.

The different schemes represent the first steps in a systematic approach to the generalization of the idea of an adjustable control variate to a vast variety of PIC simulations. The aim is a fully adaptive control variate scheme which automatically extracts a large fraction of the gyro-center distribution function to transfer it into a "noise free" analytic representation.

The organization of the paper is as follows: The $p_\parallel$-formulation of the gyrokinetic model is introduced in Section 2. The PIC discretization of the model equations leads to the inaccuracy problem (Section 3). This problem is connected to the discretization of the field equations (Section 4). The control variates method is introduced (Section 5), discretized (Section 6) and adapted to our requirements (Section 7). In Section 8, five schemes are presented which overcome the inaccuracy problem using the control variates method. The numerical results of simulations of a slab problem in the MHD limit using these schemes are presented in Section 9.

2. The gyrokinetic model

The nonlinear gyrokinetic equations in the $p_\parallel$-formulation derived from the gyrokinetic Vlasov equation [8] are used to calculate the time evolution of the gyro-center distribution function $f_s(\mathbf{R}, p_\parallel, \tilde{\mu})$ of species $s = \mathrm{i}, \mathrm{e}$ (ions and electrons)

$$\frac{\mathrm{d}f_s}{\mathrm{d}t} = \frac{\partial f_s}{\partial t} + \frac{\mathrm{d}\mathbf{R}}{\mathrm{d}t}\cdot\nabla f_s + \frac{\mathrm{d}p_\parallel}{\mathrm{d}t}\frac{\partial f_s}{\partial p_\parallel} = 0, \tag{1}$$

where $\mathbf{R}$, $p_\parallel$ and $v_\perp$ are the gyro-center position, parallel momentum per unit mass and perpendicular component of the gyro-center velocity with respect to the magnetic field direction. The magnetic moment per unit mass, $\tilde{\mu}$, of the gyro-center is given by

$$\tilde{\mu} \stackrel{\mathrm{def}}{=} \frac{v_\perp^2}{2B} \quad \text{and} \quad \frac{\mathrm{d}\tilde{\mu}}{\mathrm{d}t} = 0. \tag{2}$$

The equations of motion for the perturbed gyro-center trajectories in reduced phase-space ($\mathbf{R}$, $p_\parallel$, $\tilde{\mu}$) are

$$\frac{\mathrm{d}\mathbf{R}}{\mathrm{d}t} = \left(p_\parallel - \frac{q_s}{m_s}\langle A_\parallel\rangle_s\right)\mathbf{b}^\star - \frac{1}{q_s B_\parallel^\star}(m_s\tilde{\mu}\nabla B + q_s\nabla\langle\psi_{\mathrm{eff}}\rangle_s)\times\mathbf{e}_\mathrm{B}, \tag{3}$$

$$\frac{\mathrm{d}p_\parallel}{\mathrm{d}t} = -\tilde{\mu}\nabla B - \frac{q_s}{m_s}\nabla\langle\psi_{\mathrm{eff}}\rangle_s\cdot\mathbf{b}^\star \tag{4}$$

with ϕ and $A_\parallel$ the perturbed electrostatic and magnetic potentials, $B_\parallel^\star = \mathbf{e}_\mathrm{B}\cdot\nabla\times\mathbf{A}^\star$ and $\mathbf{b}^\star = \nabla\times\mathbf{A}^\star/B_\parallel^\star$. Here, $\mathbf{A}^\star = \mathbf{A} + (m_s p_\parallel/q_s)\mathbf{e}_\mathrm{B}$ is the so-called modified vector potential, $\mathbf{A}$ the magnetic vector potential corresponding to the equilibrium magnetic field $\mathbf{B} = \nabla\times\mathbf{A}$ and $\mathbf{e}_\mathrm{B} = \mathbf{B}/B$ its unit vector, $\Omega_{\mathrm{cs}} = q_s B/m_s$ the cyclotron frequency, and q_s and m_s the charge and mass of species s. The gyro-averaged effective potential seen by species s is defined by

$$\langle\psi_{\mathrm{eff}}\rangle_s \stackrel{\mathrm{def}}{=} \langle\phi\rangle_s - p_\parallel\langle A_\parallel\rangle_s. \tag{5}$$

The corresponding gyro-averaged potentials are defined as

$$\langle\phi\rangle_s(\mathbf{R},\tilde{\mu}) \stackrel{\mathrm{def}}{=} \frac{1}{2\pi}\oint\phi(\mathbf{R}+\boldsymbol{\rho}_s)\,\mathrm{d}\alpha, \quad \langle A_\parallel\rangle_s(\mathbf{R},\tilde{\mu}) \stackrel{\mathrm{def}}{=} \frac{1}{2\pi}\oint A_\parallel(\mathbf{R}+\boldsymbol{\rho}_s)\,\mathrm{d}\alpha, \tag{6}$$

where $\boldsymbol{\rho}_s$ is the gyro-radius vector perpendicular to $\mathbf{e}_\mathrm{B}$ which can be parameterized by the gyro-phase angle α

$$\boldsymbol{\rho}_s(\alpha) \stackrel{\mathrm{def}}{=} \rho_s[\cos(\alpha)\mathbf{e}_{\perp 1} + \sin(\alpha)\mathbf{e}_{\perp 2}] \quad \text{and} \quad \rho_s = \frac{v_\perp}{\Omega_{\mathrm{cs}}(\mathbf{R})}. \tag{7}$$

Note that we are not interested here in the actual direction of rotation of the physical particle of species s.

As long as the drifts of the unperturbed gyro-center trajectories do not lead the particles away from the flux surfaces, the flux Ψ and the particle energy per unit mass $\widetilde{E} = \tilde{\mu}B + p_\parallel^2/2$ are two invariants of the unperturbed gyro-center trajectories. We define f_0 as a local Maxwellian, a function of these invariants:

$$f_{0s}(\Psi,\widetilde{E}) \stackrel{\mathrm{def}}{=} \frac{n_{0s}(\Psi)}{(2\pi)^{3/2}v_{\mathrm{ths}}^3(\Psi)}\exp\left[-\frac{\widetilde{E}}{v_{\mathrm{ths}}^2(\Psi)}\right] \quad \text{where } v_{\mathrm{ths}}(\Psi) \stackrel{\mathrm{def}}{=} \sqrt{\frac{k_\mathrm{B}T_s(\Psi)}{m_s}}. \tag{8}$$

The quasi-neutrality equation and parallel Ampère's law close the self-consistent gyrokinetic Vlasov-Maxwell system. Using the theory of Lie transforms (see Ref. [11]) the quasi-neutrality condition and Ampère's law take under the usual assumptions of an equilibrium Maxwellian distribution f_{0s} and $q_s\langle\psi_{\mathrm{eff}}\rangle_s/(k_\mathrm{B}T_s) \ll 1$ the form:

$$-\frac{en_0}{k_\mathrm{B}T_\mathrm{i}}(\langle\bar{\phi}\rangle_\mathrm{i} - \phi) - \frac{en_0}{k_\mathrm{B}T_\mathrm{e}}(\langle\bar{\phi}\rangle_\mathrm{e} - \phi) = \langle n_\mathrm{i}\rangle - \langle n_\mathrm{e}\rangle, \tag{9}$$

$$\frac{\beta_\mathrm{i}}{\tilde{\rho}_\mathrm{i}^2}\langle\overline{A}_\parallel\rangle_\mathrm{i} + \frac{\beta_\mathrm{e}}{\tilde{\rho}_\mathrm{e}^2}\langle\overline{A}_\parallel\rangle_\mathrm{e} - \nabla_\perp^2 A_\parallel = \mu_0(\langle j_{\parallel\mathrm{i}}\rangle + \langle j_{\parallel\mathrm{e}}\rangle), \tag{10}$$

where

$$\langle n_s\rangle(\mathbf{x}) \stackrel{\text{def}}{=} \int f_s(\mathbf{R}, p_\parallel, \tilde{\mu})\delta(\mathbf{R}+\boldsymbol{\rho}_s-\mathbf{x})\,\mathrm{d}^6Z, \tag{11}$$

$$\langle j_{\parallel s}\rangle(\mathbf{x}) \stackrel{\text{def}}{=} q_s \int p_\parallel f_s(\mathbf{R}, p_\parallel, \tilde{\mu})\delta(\mathbf{R}+\boldsymbol{\rho}_s-\mathbf{x})\,\mathrm{d}^6Z \tag{12}$$

are the number and current density represented by the gyro-center distribution function f_s in the $p_\parallel$-formulation. The integration is performed over phase-space $\mathrm{d}^6Z = B_\parallel^\star \mathrm{d}\mathbf{R}\mathrm{d}p_\parallel \mathrm{d}\tilde{\mu}\mathrm{d}\alpha$. The thermal gyro-radius is $\tilde{\rho}_s = \sqrt{m_s k_\mathrm{B} T_s}/(q_s B)$, the plasma beta corresponding to the particular species is $\beta_s = \mu_0 n_0 k_\mathrm{B} T_s/B^2$ and the potentials averaged over the gyro-phase and over the Maxwellian background are defined as

$$\langle\bar{\phi}\rangle_s \stackrel{\text{def}}{=} \frac{1}{n_0(\mathbf{x})}\int f_{0s}(\mathbf{R}, p_\parallel, \tilde{\mu})\langle\phi\rangle_s\delta(\mathbf{R}+\boldsymbol{\rho}_s-\mathbf{x})\,\mathrm{d}^6Z, \tag{13}$$

$$\langle\overline{A}_\parallel\rangle_s \stackrel{\text{def}}{=} \frac{1}{n_0(\mathbf{x})}\int f_{0s}(\mathbf{R}, p_\parallel, \tilde{\mu})\langle A_\parallel\rangle_s\delta(\mathbf{R}+\boldsymbol{\rho}_s-\mathbf{x})\,\mathrm{d}^6Z. \tag{14}$$

We assume here that the ion charge $q_\mathrm{i} = e$ and the electron charge $q_\mathrm{e} = -e$ have the same absolute values. Hence, the ion and electron equilibrium densities are equal $n_{0\mathrm{i}} = n_{0\mathrm{e}} = n_0$.

A long-wavelength approximation can be applied to the quasi-neutrality condition Eq. (9), and Ampère's law, Eq. (10). This leads to the gyro-dependent quantities of the ion gyro-average in Eqs. (13) and (14) being expanded in Fourier space up to the order of $\mathrm{O}(k_\perp\tilde{\rho}_\mathrm{i})^2$, and the finite gyro-radius effects being neglected for the electrons. Under this approximation the quasi-neutrality condition and Ampère's law take the following form:

$$-\nabla_\perp\cdot\left(\frac{en_0}{k_\mathrm{B}T_\mathrm{i}}\tilde{\rho}_\mathrm{i}^2\nabla_\perp\phi\right) = \langle n_\mathrm{i}\rangle - n_\mathrm{e}, \tag{15}$$

$$\frac{\beta_\mathrm{i}}{\tilde{\rho}_\mathrm{i}^2}A_\parallel + \frac{\beta_\mathrm{e}}{\tilde{\rho}_\mathrm{e}^2}A_\parallel - \nabla_\perp\cdot[(1-\beta_\mathrm{i})\nabla_\perp A_\parallel] = \mu_0(\langle j_{\parallel\mathrm{i}}\rangle + j_{\parallel\mathrm{e}}). \tag{16}$$

3. The inaccuracy problem

On the left-hand-side of Ampère's law, Eq. (10), we have the ion and electron skin terms:

$$\frac{\beta_\mathrm{i}}{\tilde{\rho}_\mathrm{i}^2}\langle\overline{A}_\parallel\rangle_\mathrm{i} = \frac{\mu_0 e^2 n_0}{m_\mathrm{i}}\langle\overline{A}_\parallel\rangle_\mathrm{i} \quad\text{and}\quad \frac{\beta_\mathrm{e}}{\tilde{\rho}_\mathrm{e}^2}\langle\overline{A}_\parallel\rangle_\mathrm{e} = \frac{\mu_0 e^2 n_0}{m_\mathrm{e}}\langle\overline{A}_\parallel\rangle_\mathrm{e}, \tag{17}$$

where especially the electron skin term is large due to the small electron mass in the denominator. The adiabatic part of the distribution function δf_s^{ad} for the effective potential $\langle\psi_{\mathrm{eff}}\rangle_s$ is

$$\delta f_s^{\mathrm{ad}} = -\frac{q_s f_{0s}}{k_\mathrm{B}T_s}\langle\psi_{\mathrm{eff}}\rangle_s \tag{18}$$

which is related to the δf_e ansatz of the split-weight scheme of Ref. [6].

We split the currents on the right-hand-side of Ampère's law into their adiabatic and nonadiabatic parts using Eq. (18) and the definition of the current density, Eq. (12):

$$\langle j_{\parallel s}\rangle = \langle j_{\parallel s}\rangle^{\mathrm{ad}} + \langle j_{\parallel s}\rangle^{\mathrm{nonad}} \quad\text{with}\quad \langle j_{\parallel s}\rangle^{\mathrm{ad}} = \frac{q_s^2}{k_\mathrm{B}}\int\frac{p_\parallel^2 f_{0s}}{T_s}\langle A_\parallel\rangle_s\delta(\mathbf{R}+\boldsymbol{\rho}_s-\mathbf{x})\,\mathrm{d}^6Z. \tag{19}$$

Now, we see that the adiabatic current terms coincide with the skin terms in Eq. (17) which is a direct consequence of the $p_\parallel$-formulation:

$$\mu_0\langle j_{\parallel s}\rangle^{\mathrm{ad}} = \frac{\mu_0 n_0 q_s^2}{m_s}\langle\overline{A}_\parallel\rangle_s = \frac{\beta_s}{\tilde{\rho}_s^2}\langle\overline{A}_\parallel\rangle_s. \tag{20}$$

In other words, the skin terms on the left-hand-side of Ampère's law, Eq. (10), cancel with the adiabatic currents on the right-hand-side. Accordingly, only the nonadiabatic currents represent the physics:

$$-\nabla_\perp^2 A_\parallel = \mu_0(\langle j_{\parallel \mathrm{i}}\rangle^{\mathrm{nonad}} + \langle j_{\parallel \mathrm{e}}\rangle^{\mathrm{nonad}}). \tag{21}$$

If the numerical discretization of the currents has to represent both the adiabatic and nonadiabatic part, the adiabatic part will become the dominant for the high beta case, $\beta \approx 1\%$, and/or the magnetohydrodynamic (MHD) limit $k_\perp \to 0$. This can be seen by the ratio of the adiabatic and nonadiabatic currents:

$$\frac{\langle j_{\parallel \mathrm{e}}\rangle^{\mathrm{ad}}}{\langle j_{\parallel \mathrm{i}}\rangle^{\mathrm{nonad}} + \langle j_{\parallel \mathrm{e}}\rangle^{\mathrm{nonad}}} \approx \frac{\beta_\mathrm{e}/\tilde{\rho}_\mathrm{e}^2 \langle \overline{A}_\parallel\rangle_\mathrm{e}}{\nabla_\perp^2 A_\parallel}. \tag{22}$$

While the adiabatic electron current scales linearly with β_e, the nonadiabatic part scales with $k_\perp^2$ which makes the MHD limit $k_\perp \to 0$ the most challenging case for PIC methods. The nonadiabatic part is a small fraction of the total current, easily swamped by the discretization error unless the noise is made very small (requiring a very large number of markers). However, the presence of a dominant adiabatic electron current implies the presence of a dominant part responding adiabatically to the magnetic potential $\langle A_\parallel\rangle_\mathrm{e}$ in the perturbation of the distribution function of the electrons:

$$\delta f_\mathrm{e}^{\mathrm{ad}} \approx -\frac{e p_\parallel f_{0\mathrm{e}}}{k_\mathrm{B} T_\mathrm{e}} \langle A_\parallel\rangle_\mathrm{e}. \tag{23}$$

It is important to note that this causes not only an inaccuracy problem when calculating the electron current density $\langle j_{\parallel \mathrm{e}}\rangle$ in Ampère's law but also in the calculation of the electron number density $\langle n_\mathrm{e}\rangle$ in the quasi-neutrality equation.

As a consequence of the $p_\parallel$-formalism, there is an additional term

$$-\frac{e}{k_\mathrm{B}} \int \frac{p_\parallel f_{0\mathrm{e}}}{T_\mathrm{e}} \langle A_\parallel\rangle_\mathrm{e} \delta(\mathbf{R} + \boldsymbol{\rho}_\mathrm{e} - \mathbf{x})\, \mathrm{d}^6 Z = 0 \tag{24}$$

on the right-hand-side of the quasi-neutrality equation, Eq. (9), which is usually not printed as analytically it gives no contribution to the number density. However, the integrand can take large absolute values due to the fast electron motion (large parallel momentum $p_\parallel$), which is a result of the small electron mass. Hence, if this integral is calculated statistically by a discretization of N_e electron markers a potentially large statistical error $\epsilon(N_\mathrm{e})$ results from the discretization of the number density. As the integrand is proportional to the absolute value of the magnetic potential, the statistical error ϵ will increase with increasing $\langle A_\parallel\rangle_\mathrm{e}$. Although the inaccuracy problem in the quasi-neutrality equation is not as obvious as in Ampère's law it has the same origin as the cancellation problem.

4. Galerkin's method in PIC applications

Considering the discretization of a function $h(\mathbf{x})$ with finite elements, we want to review here on the very basics of Galerkin's method. A detailed introduction can be found e.g. in Ref. [12]. The discretization of $h(\mathbf{x})$ is given by

$$u(\mathbf{x}) = \sum_{j=1}^{M} \hat{c}_j \Lambda_j(\mathbf{x}), \tag{25}$$

where the finite element basis consists of the elements $\Lambda_j(\mathbf{x})$. Supposed that a scalar product is defined by

$$(u, v) \stackrel{\mathrm{def}}{=} \int u(\mathbf{x}) v(\mathbf{x})\, \mathrm{d}\mathbf{x} \tag{26}$$

the Galerkin approach requires

$$(u - h, \Lambda_j) = 0 \Rightarrow (u, \Lambda_j) = (h, \Lambda_j) \quad \forall \Lambda_j. \tag{27}$$

This can be expressed by the Galerkin matrix equation

$$\sum_{j=1}^{M} \hat{a}_{kj} \hat{c}_j = \hat{b}_k \quad k = 1, \ldots, M, \tag{28}$$

where the mass matrix $\widehat{\mathbf{A}}$ and load vector $\hat{\mathbf{b}}$ are defined as

$$\hat{a}_{kj} \stackrel{\text{def}}{=} \int \Lambda_j(\mathbf{x})\Lambda_k(\mathbf{x})\,\mathrm{d}\mathbf{x} \quad \text{and} \quad \hat{b}_k \stackrel{\text{def}}{=} \int h(\mathbf{x})\Lambda_k(\mathbf{x})\,\mathrm{d}\mathbf{x}. \tag{29}$$

Essentially the load vector can be interpreted as the projection of the function $h(\mathbf{x})$ onto the subspace spanned by the finite element basis.

After solving the Galerkin matrix equation, Eq. (28), for $\hat{c}$ the function $u(\mathbf{x})$ is well defined at every point in the domain (see Eq. (25)). Operators like integrals and derivatives acting on $u(\mathbf{x})$ can be performed by just letting them act on the elements $\Lambda_j(\mathbf{x})$ of the finite element basis. As direct consequence the finite element discretization gives an energy-conserving scheme [13,14] due to the well-defined gradient in the force calculation. Complex geometries can be handled by appropriate coordinate systems (e.g. polar coordinates) so that the geometrical issues are only a matter of the corresponding calculus of the finite elements $\Lambda_j(\mathbf{x})$ as can be seen e.g. by the Jacobian of the integrals in Eq. (29).

The Galerkin approach is used e.g. in PIC simulations to discretize the number density which is defined as a moment of the gyro-center distribution function $f(\mathbf{R},\mathbf{v})$. If e.g. the number density should be evaluated for a drift-kinetic charge-assignment, the load vector would be defined by the following integral over space and velocity coordinates

$$\check{b}_k \stackrel{\text{def}}{=} \int\int f(\mathbf{R},\mathbf{v})\delta(\mathbf{R}-\mathbf{x})\Lambda_k(\mathbf{x})\,\mathrm{d}\mathbf{R}\,\mathrm{d}\mathbf{v}\,\mathrm{d}\mathbf{x}. \tag{30}$$

Note that the shape factor (particle cloud) of the markers $\Lambda_k(\mathbf{x})$ is a natural consequence of the finite element formalism.

Formally, one has to distinguish between the gyro-center coordinate $\mathbf{R}$ of the gyro-center distribution function and the spatial coordinate $\mathbf{x}$ which requires the usage of the δ function in Eq. (30). However, in Sections 6 and 7 we will not make this distinction as we only consider the case of a drift-kinetic charge-assignment. Nevertheless, for a gyrokinetic charge-/current-assignment the difference is crucial and will be handled with care in the Appendices A and C.

Furthermore, in PIC simulation the gyro-center distribution is represented by a sum over δ functions at the marker positions [15,16]

$$\hat{f}(\mathbf{R},p_\parallel,\tilde{\mu}) \stackrel{\text{def}}{=} \sum_{p=1}^{N} w_p\delta^3[\mathbf{R}-\mathbf{R}_p(t)]\delta[p_\parallel - p_{\parallel p}(t)]\delta[\tilde{\mu}-\tilde{\mu}_p(t_0)]/[2\pi B_\parallel^\star(\mathbf{R},p_\parallel)]. \tag{31}$$

Let us define f_p as the distribution function f averaged over the phase space volume Ω_p centered initially around a marker p:

$$f_p \stackrel{\text{def}}{=} \frac{2\pi}{\Omega_p}\int_{\Omega_p} f(\mathbf{R},p_\parallel,\tilde{\mu})B^\star(\mathbf{R},p_\parallel)\,\mathrm{d}\mathbf{R}\,\mathrm{d}p_\parallel\,\mathrm{d}\tilde{\mu}. \tag{32}$$

Approximating f in the integrand as $\hat{f}$ from Eq. (31) and using Liouville's theorem for the constancy of Ω_p we find the relationship between f_p and the weight w_p of marker p at the position $(\mathbf{R}=\mathbf{R}_p, p_\parallel = p_{\parallel p}, \tilde{\mu}=\tilde{\mu}_p)$:

$$w_p = \Omega_p f_p. \tag{33}$$

The weights represent the number of physical particles contained in the volume Ω_p of marker p and are constant in time for nonlinear collisionless gyrokinetic simulation, Eq. (1).

Inserting the discrete approximation of f from Eq. (31) into Eq. (30) the load vector or charge-assignment vector is now defined by

$$b_k \stackrel{\text{def}}{=} \sum_{p=1}^{N_s} w_p\Lambda_k(\mathbf{x}_p). \tag{34}$$

Hence, the charge-assignment procedure can be interpreted as a projection of a sum of δ functions onto the subspace spanned by the finite elements. The atomic process consists of the projection of each δ function at the marker position onto the finite element basis. Usually, the finite element basis is only able to produce a poor approximation of the δ function which could give due to aliasing even negative values in some regions of space. The more markers we use, the better these undesired approximation effects cancel out each other.

However, we have to question the approximation of the gyro-center distribution function by a sum over δ functions. Even for smooth distribution functions the approximation gets very spiky and cannot be expressed properly by the finite element basis. Instead, we have to reinterpret the charge-assignment procedure as a sampling process of a smooth function at the marker positions in phase-space. Hence, we have to take into account the information about the smoothness of the distribution function into the charge-assignment procedure.

In the following, this information will be included in the PIC simulation using the control variates method. It provides the possibility to transfer part of the distribution function into an analytic representation. It guarantees that the derived algorithm is still convergent in the sense that it converges to the correct result for a sufficiently large number of markers. But with a properly chosen control variate the convergence rate can be significantly improved. In addition, the control variates method can be enhanced to fit to a certain extent to the evolving gyro-center distribution function but it has to be assured by e.g. a least square fit procedure that no noise is introduced by this adaptation process.

5. The control variates method

The key idea of the control variates method is to replace as much of the Monte Carlo estimate (the weights) as possible by analytic or numerical calculations that are more accurate (see Ref. [3]). In the following, we show how this can be done under the "direct δf" method.

The right-hand-side of the quasi-neutrality equation, Eq. (9), can be rewritten in the form:

$$\langle n_\mathrm{i}\rangle - \langle n_\mathrm{e}\rangle = \bar{n}_{0\mathrm{i}} + \underbrace{\langle n_\mathrm{i}\rangle - \bar{n}_{0\mathrm{i}}}_{\delta\langle n_\mathrm{i}\rangle} - (\bar{n}_{0\mathrm{e}} + \underbrace{\langle n_\mathrm{e}\rangle - \bar{n}_{0\mathrm{e}}}_{\delta\langle n_\mathrm{e}\rangle}) = \underbrace{\bar{n}_{0\mathrm{i}} - \bar{n}_{0\mathrm{e}}}_{\text{analytical}} + \underbrace{\delta\langle n_\mathrm{i}\rangle - \delta\langle n_\mathrm{e}\rangle}_{\text{statistical}}. \tag{35}$$

The n_{0s} terms calculated from the local Maxwellian f_{0s} of species s are analytically known, they can be represented directly in the finite element basis. The δn_s terms are the result of the PIC simulation and are calculated statistically in the charge-assignment procedure, Eq. (34), of the weights. The magnitude of the statistical error inherent in the weight representation is proportional to the "size" of the distribution function represented. Hence, the decomposition, Eq. (35), is only advantageous if the perturbed distribution functions $\delta f_s = f_s - f_{0s}$ sampled for the calculation of the perturbed number densities $\delta\bar{n}_s$ (the charge-assignment procedure) are much smaller than the full distribution functions f_s, in the sense $\|\delta f_s\|/\|f_s\| \ll 1$.

To take advantage of the control variates method the perturbed distribution functions δf_s have to be known to compute the δn_s in Eq. (35). Thus, the weights w_{sp} of species s which are constant in time have to be diminished by the contribution of the (additive) control variate, the function $\bar{f}_s = f_{0s}$, just for the charge-assignment to become "noise reduced" weights:

$$\bar{w}_{sp}(t) \stackrel{\mathrm{def}}{=} \Omega_{sp}[f_s(\mathbf{R}_p(t_0), p_{\|p}(t_0)) - f_{0s}(\mathbf{R}_p, p_{\|p})] = w_{sp} - \Omega_{sp} f_{0s}(t). \tag{36}$$

The time-dependent positions of the markers along the perturbed trajectories of the gyro-centers determine the value of $f_{0s}(t)$ and consequently of δf_s needed for the noise reduction. In the framework of the control variates method, we establish a noise reduced "direct δf" method identical to the method proposed in Refs. [3,17,18].

However, the "direct δf" method can be used only for nonlinear simulation as the markers have to follow the perturbed trajectories. Linear simulation uses the δf_s ansatz

$$f_s(\mathbf{R}, p_\|, \tilde{\mu}, t) \stackrel{\mathrm{def}}{=} f_{0s}(\mathbf{R}, p_\|, \tilde{\mu}) + \delta f_s(\mathbf{R}, p_\|, \tilde{\mu}, t) \tag{37}$$

in Eq. (1) and leads to the evolution equation for the perturbation to the distribution function δf_s along the unperturbed gyro-center trajectories of species s

$$\left.\frac{\mathrm{d}}{\mathrm{d}t}\right|_0 \delta f_s = -\left.\frac{\mathrm{d}}{\mathrm{d}t}\right|_0 f_{0s} - \left.\frac{\mathrm{d}}{\mathrm{d}t}\right|_1 f_{0s} = -\left.\frac{\mathrm{d}}{\mathrm{d}t}\right|_1 f_{0s}, \tag{38}$$

where f_{0s} is an exact solution of the unperturbed Vlasov equation $\mathrm{d}f_{0s}/\mathrm{d}t|_0 = 0$. For the GYGLES code [15] which uses e.g. the gyro-center coordinates $(\mathbf{R}, p_\|, v_\perp)$ the corresponding evolution equation for δf is given by

$$\left.\frac{\mathrm{d}}{\mathrm{d}t}\right|_0 \delta f_s = \left(\frac{\nabla\langle\psi_{\mathrm{eff}}\rangle_s \times \mathbf{e}_{\mathrm{B}}}{B_{\parallel}^{\star}} + \frac{q_s}{m_s}\langle A_{\parallel}\rangle_s \mathbf{b}^{\star}\right)\left(\frac{\partial f_{0s}}{\partial \mathbf{R}} + \frac{v_{\perp}\nabla B}{2B}\frac{\partial f_{0s}}{\partial v_{\perp}}\right) + \frac{q_s}{m_s}\nabla\langle\psi_{\mathrm{eff}}\rangle_s \cdot \mathbf{b}^{\star}\frac{\partial f_{0s}}{\partial p_{\parallel}}. \tag{39}$$

Integrating this equation, we can evolve the weights of the markers $w_{sp} = \Omega_{sp}\delta f_s(t)$ which are time-dependent and have already the property of being "noise reduced", $\bar{w}_{sp} = w_{sp}$, as they evolve only the perturbation to the particle number.

We have shown that the control variates method is used for both, the "direct δf" and the δf method. In a further step, it can be enhanced to solve the inaccuracy problem described in Section 3. In contrast to the split-weight scheme which actually splits the δf_{e} ansatz of the electrons by introducing a time dependent control variate, the evolution equation of δf_s, Eq. (39), is not modified. Instead, the weights of the electron markers are adapted (split) exclusively for the charge-/current-assignment so that only at this step a third, further "noise reduced" species of weights

$$\hat{w}_{sp} = \Omega_{sp}\{\delta f_s(t^n) - \bar{f}_s[\delta f_s(t^n)]\} \tag{40}$$

is introduced. Here, $\bar{f}_s[\delta f_s(t^n)]$ is a control variate chosen exclusively for a certain point in time t^n which has the capability to be adjusted to a certain extent to the perturbation to the distribution function $\delta f_s(t^n)$.

6. The discretization of the control variates method with Galerkin's method

In the following sections we discretize the control variates method for just one particle species s. If more than one particle species is present, e.g. ions and electrons, the control variates method would have to be applied separately for each gyro-center distribution function f_s. Also to simplify matters, we will discretize the control variates method by means of the charge-assignment procedure although its application will be in Section 8 for both the charge- and current-assignment.

Let us suppose that the control variate $\bar{f}$ is defined as a product ansatz

$$\bar{f}(\mathbf{x},\mathbf{v}) \overset{\mathrm{def}}{=} g(\mathbf{x},\mathbf{v})\sum_{j=1}^{M} c_j B_j^d(\mathbf{x}) \quad \text{with} \quad \int_0^{\infty} g(\mathbf{x},\mathbf{v})\,\mathrm{d}\mathbf{v} = 1, \quad g(\mathbf{x},\mathbf{v}) \neq 0, \tag{41}$$

where $B_j^d(\mathbf{x})$ is a product of 1-D B-splines of order d (tensor product B-splines, see e.g. Ref. [12]). A suitable choice for e.g. a three dimensional discretization of a slab would be in Cartesian coordinates (x, y, z):

$$B_j^d(\mathbf{x}) = S_a^d(x)S_b^d(y)S_c^d(z), \tag{42}$$

where the index j stands for the triplet (a, b, c) of indices. The boundary conditions would be Dirichlet in x-direction, and periodic in y- and z-direction which can be easily implemented in the finite element formalism (see e.g. Ref. [19]) on each dimension separately. Even complicated physical domains as e.g. stellarators have been discretized with tensor product B-splines [20]. The B-spline sequence (B_j^d) consists of nonnegative functions which sum to 1, i.e. in mathematical terms, (B_j^d) provides a partition of unity (see Ref. [19], p. 111), which guarantees the conservation of particle number in the charge-assignment.

The coefficient vector $\mathbf{c}$ is used to adjust the control variate. For instance, it can be used to represent the density n_0 as it is the case for the conventional δf method where a local Maxwellian, Eq. (8), is used as the control variate

$$n_0(\Psi) = \sum_{j=1}^{M} c_j B_j^d(\mathbf{x}) \quad \text{and} \quad g(\Psi,\tilde{v}) \overset{\mathrm{def}}{=} \frac{\exp(\tilde{v})}{(2\pi)^{3/2}v_{\mathrm{th}}^3(\Psi)}, \quad \tilde{v} \overset{\mathrm{def}}{=} -\frac{\widetilde{E}}{v_{\mathrm{th}}^2(\Psi)}. \tag{43}$$

Using a B-spline finite element basis for the discretization of the quasi-neutrality equation, the charge-assignment vector can be rewritten with the control variates method, Eq. (35), discretizing the analytical and statistical part corresponding to Eqs. (30) and (34)

$$\tilde{b}_k = \int\int \bar{f}_p B_k^d(\mathbf{x})\,\mathrm{d}\mathbf{x}\,\mathrm{d}\mathbf{v} + \sum_{p=1}^{N_s}(f_p - \bar{f}_p)B_k^d(\mathbf{x}_p)\Omega_p = \bar{b}_k + \delta b_k. \tag{44}$$

The contribution of the control variate $\bar{f}$ to the charge-assignment can be written explicitly with two matrix equations. Firstly, the contribution of the control variate itself

$$\bar{\mathbf{b}} = \widehat{\mathbf{A}}\mathbf{c}, \tag{45}$$

where one finds again the mass matrix, Eq. (29), defined as $M \times M$ matrix

$$\hat{a}_{kj} \stackrel{\text{def}}{=} \int_0^\infty \left[\int B_j^d(\mathbf{x}) B_k^d(\mathbf{x}) g(\mathbf{x}, \mathbf{v}) \, \mathrm{d}\mathbf{x} \right] \mathrm{d}\mathbf{v} = \int B_j^d(\mathbf{x}) B_k^d(\mathbf{x}) \, \mathrm{d}\mathbf{x} \tag{46}$$

which is independent of the $(\mathbf{x}_p, \mathbf{v}_p)$ positions of the markers. Its matrix elements can be calculated e.g. numerically with a Gaussian quadrature formula even for complicated geometrical configurations.

Secondly, the charge-assignment of the marker weights diminished by the contribution of the control variate at the marker position is

$$\delta b_k = \sum_{p=1}^{N_s} (f_p - \bar{f}_p) \Omega_p B_k^d(\mathbf{x}_p) = \sum_{p=1}^{N_s} \left[f_p - g(\mathbf{x}_p, \mathbf{v}_p) \sum_{j=1}^{M} c_j B_j^d(\mathbf{x}_p) \right] \Omega_p B_k^d(\mathbf{x}_p) \tag{47}$$

which can be written in the form of a matrix equation:

$$\boldsymbol{\delta}\mathbf{b} = \mathbf{b} - \mathbf{A}\mathbf{c}, \tag{48}$$

where

$$a_{kj} \stackrel{\text{def}}{=} \sum_{p=1}^{N_s} B_j^d(\mathbf{x}_p) B_k^d(\mathbf{x}_p) g(\mathbf{x}_p, \mathbf{v}_p) \Omega_p \tag{49}$$

$$b_k \stackrel{\text{def}}{=} \sum_{p=1}^{N_s} \Omega_p f_p B_k^d(\mathbf{x}_p) = \sum_{p=1}^{N_s} w_p B_k^d(\mathbf{x}_p). \tag{50}$$

The matrix $\mathbf{A}$ will be called henceforth the diminishing matrix and it obviously depends on the $(\mathbf{x}_p, \mathbf{v}_p)$ position of the markers. In principle, it has to be constructed for each call of the charge-assignment procedure again.

Inserting Eqs. (45) and (48) into Eq. (44) we finally achieve for the charge-assignment vector

$$\tilde{\mathbf{b}} = \widehat{\mathbf{A}}\mathbf{c} + \mathbf{b} - \mathbf{A}\mathbf{c} = (\widehat{\mathbf{A}} - \mathbf{A})\mathbf{c} + \mathbf{b}. \tag{51}$$

The scheme must be consistent in the sense that, for an infinite number of markers it must give $\tilde{\mathbf{b}} = \mathbf{b}$. Hence, the integration over the velocity sphere in Eq. (46) has to be consistent with the discretization limit of the velocity sphere of the markers. In our simulations, we distribute the markers in a velocity sphere limited by $v_{\max} = \kappa_v v_{\text{th}}$. In the case of $\bar{f} = f_0$, Eq. (46) has to be recalculated:

$$\hat{a}_{kj} = \int_0^{v_{\max}} \left[\int B_j^d(\mathbf{x}) B_k^d(\mathbf{x}) g(\mathbf{x}, \mathbf{v}) \, \mathrm{d}\mathbf{x} \right] \mathrm{d}\mathbf{v} = C_{\text{v1}} \int B_j^d(\mathbf{x}) B_k^d(\mathbf{x}) \, \mathrm{d}\mathbf{x}, \tag{52}$$

where

$$C_{\text{v1}}(\kappa_v) \stackrel{\text{def}}{=} \operatorname{erf}\left(\frac{\kappa_v}{\sqrt{2}} \right) - \sqrt{\frac{2}{\pi}} \kappa_v \exp\left(-\frac{\kappa_v^2}{2} \right). \tag{53}$$

The generalization of the scheme derived in Eq. (51) for a gyro-averaged charge-assignment can be found in Appendix A.

7. Adjustable control variates methods

In principle, one is completely free in the choice of the control variate. However, it is worth remarking that a poorly chosen control variate can be worse than ineffective as it can lead to an increased statistical noise level (for details see e.g. Ref. [21]). For evaluation purpose we define a quality measure σ of the control variate $\bar{f}$ as follows:

$$\sigma \stackrel{\text{def}}{=} \sqrt{\frac{\sum_{p=1}^{N_s}[\tau_p(f_p - \bar{f}_p)]^2}{\sum_{p=1}^{N_s}(\tau_p f_p)^2}}. \tag{54}$$

The weighting factor τ_p specifies if the quality measure is used either to evaluate a control variate for a charge-assignment $\tau_{\text{den}p} = \Omega_p$ or a current-assignment $\tau_{\text{cur}p} = p_{\|p}\Omega_p$. The quality measure gives us the possibility to quantify how close the control variate fits the gyro-center distribution function f and it should be $\sigma \ll 1$ for an effective control variate with noise reduction property.

We will use now the degree of freedom of the B-spline representation in our control variate, Eq. (41),

$$f_{\text{adj}}(\mathbf{x}) \stackrel{\text{def}}{=} \sum_{j=1}^{M} c_j B_j^d(\mathbf{x}) \tag{55}$$

to construct a control variate $\bar{f}$ being adjusted to the gyro-center distribution function at each call of the charge-assignment procedure.

If one has access to additional information about the structure of the gyro-center distribution function, it is possible to use an heuristic approach for the construction of an adjustable control variate scheme. For instance, the information could come from the knowledge of the equilibrium distribution function as e.g. for the δf method or it could come from the formalism used to derive the model equations or, even that is possible, just intuition.

As an example, one could suppose for ion-temperature-gradient driven (ITG) mode simulation in the electrostatic limit the presence of a dominant part responding adiabatically to the electrostatic potential ϕ in the perturbation of the distribution function $\delta f_e(\mathbf{R}, p_\|, \tilde{\mu})$ of the electrons. Hence, the resulting control variate would be adjusted by the electrostatic potential ϕ

$$\bar{f}_{e1}(\mathbf{x}, \mathbf{v}) \stackrel{\text{def}}{=} -\frac{en_0}{k_B T_e} f_{\text{adj}1}(\mathbf{x}) g_1(\Psi, \tilde{v}), \tag{56}$$

where

$$f_{\text{adj}1}(\mathbf{x}) = \phi(\mathbf{x}) = \sum_{j=1}^{M} c_j^{(1)} B_j^d(\mathbf{x}), \quad g_1(\Psi, \tilde{v}) \stackrel{\text{def}}{=} \frac{\exp(\tilde{v})}{(2\pi)^{3/2} v_{\text{the}}^3(\Psi)}. \tag{57}$$

The construction of the corresponding scheme would be analog to the derivation given in Section 8.2 for electromagnetic simulation.

In addition, we present two systematic approaches to derive the adjustable part, Eq. (55), of the control variate:

(1) We construct a scheme herein after referred to as the moment adjusting scheme which determines the adjustable part by the moments of the distribution function e.g. the number and/or current density. For the derivation of its control variate we suppose that the product ansatz of the control variate, Eq. (41), fits the gyro-center distribution function perfectly which is equivalent to set $\boldsymbol{\delta}\mathbf{b} = 0$ in Eq. (48). Thus, the adjustable part of the control variate, the coefficient vector $\mathbf{c}$, is determined by the charge-assignment vector $\mathbf{b}$

$$\mathbf{A}\mathbf{c} = \mathbf{b} \Rightarrow \mathbf{c} = \mathbf{A}^{-1}\mathbf{b}. \tag{58}$$

Inserting the coefficient vector $\mathbf{c}$ into Eq. (51) we derive:

$$\tilde{\mathbf{b}} = (\widehat{\mathbf{A}} - \mathbf{A})\mathbf{A}^{-1}\mathbf{b} + \mathbf{b} = \widehat{\mathbf{A}}\mathbf{A}^{-1}\mathbf{b}. \tag{59}$$

One can see again that in the limit of an infinite number of markers the derived scheme is consistent in the sense $\tilde{\mathbf{b}} = \mathbf{b}$ as it is the case for Eq. (51). In Appendix B we will present an efficient iterative algorithm to calculate the charge-assignment vector $\tilde{\mathbf{b}}$.

(2) We construct a scheme herein after referred to as the least square fit scheme by adapting the control variate in such a way that the quality measure σ, Eq. (54), is minimized. This is done by just minimizing the numerator

$$\chi^2 = \sum_{p=1}^{N_s} \tau_p^2 (f_p - \bar{f}_p)^2 = \sum_{p=1}^{N_s} \tau_p^2 \left[f_p - g(\mathbf{x}_p, \mathbf{v}_p) \sum_{j=1}^{M} c_j B_j^d(\mathbf{x}_p) \right]^2 \to \text{Min.} \tag{60}$$

The minimization is equivalent to a least square fit procedure to find the best-fitting curve to a given set of data points by minimizing the sum of the squares of the offsets of the points from the curve. It is important to note that there is a close connection between the minimization of χ^2 and the minimization of the statistical error in PIC simulations. For instance, for nonlinear δf simulation χ with $\tau_p = \Omega_p$ is proportional to the error of the particle number conservation (see Ref. [3]). The minimization gives the following least square fit matrix equation

$$\mathbf{T}\mathbf{c} = \mathbf{r}, \tag{61}$$

where

$$t_{kj} \stackrel{\text{def}}{=} \sum_{p=1}^{N_s} \tau_p^2 B_j^d(\mathbf{x}_p) B_k^d(\mathbf{x}_p) g^2(\mathbf{x}_p, \mathbf{v}_p) \tag{62}$$

$$r_k \stackrel{\text{def}}{=} \sum_{p=1}^{N_s} \tau_p^2 f_p B_k^d(\mathbf{x}_p) g(\mathbf{x}_p, \mathbf{v}_p). \tag{63}$$

Inserting again the coefficient vector $\mathbf{c}$, Eq. (61), into Eq. (51) we derive:

$$\tilde{\mathbf{b}} = (\widehat{\mathbf{A}} - \mathbf{A})\mathbf{T}^{-1}\mathbf{r} + \mathbf{b}. \tag{64}$$

The assembly of the least square fit matrix $\mathbf{T}$ depends on the positions $(\mathbf{x}_p, \mathbf{v}_p)$ of the markers and has to be built up for each call to the charge-/current-assignment procedure again. Only then, the least square fit matrix equation, Eq. (61), can be either solved by a direct or iterative method.

Note that if the gyro-center distribution function f could be expressed exactly by the control variate $\bar{f}$ of the previous methods, there would be no longer a discretization error introduced by the charge-assignment procedure at all. In such a case, the quality measure would be $\sigma = 0$. However, a significant noise reduction could be still expected in all cases where the product ansatz, Eq. (41), is a good approximation to the gyro-center distribution function f which can be tested by $\sigma \ll 1$.

The aspects of the derived schemes in connection with the gyro-averaging process will be considered in Appendix C.

8. Cancellation schemes for Ampère's law

It is possible to perform electromagnetic PIC simulations with a conventional δf-approach in slab geometry using a B-spline discretization (see Ref. [4]). However, the required number of markers can be so large that such PIC simulations become impractical. In this section five schemes are developed with the purpose to overcome the inaccuracy problem described in Section 3. They are based on variations of the control variates method (see Section 7) and can be seen as supplements to the δf-discretization using B-splines. A concise summary of the schemes and their concepts is given in Table 1.

Table 1
Concise summary of the derived schemes in Section 8

Scheme	Section	Control variate	Iterative	Concept
δf	8.1	n_0	–	n_0 cancellation
1	8.2	$n_0 + A_\parallel(t^n)$	No	$j_{\parallel e}^{ad}$ cancellation
2	8.2	$n_0 + A_\parallel(t^n)$	Yes	$j_{\parallel e}^{ad}$ cancellation
3	8.3	$n_0 + j_{\parallel e}(t^n)$	No	Moment adjusting
4	8.3	$n_0 + j_{\parallel e}(t^n)$	Yes	Moment adjusting
5	8.4	$n_0 + A_\parallel(t^n)$	No	Least square fit

8.1. The conventional δf scheme for Ampère's law

A standard δ*f* discretization of Ampère's law in the long-wavelength approximation, Eq. (16), with B-splines would be (see e.g. Ref. [4]):

$$(\widehat{\mathbf{L}} + \widehat{\mathbf{S}}_\mathrm{i} + \widehat{\mathbf{S}}_\mathrm{e})\mathbf{c} = \mu_0(\langle \mathbf{j}_\mathrm{i}\rangle + \mathbf{j}_\mathrm{e}), \tag{65}$$

where the matrices are defined as

$$\hat{l}_{kj} \stackrel{\mathrm{def}}{=} \int (1 - C_{\mathrm{v}2}\beta_\mathrm{i})\nabla_\perp B_j^d(\mathbf{x}) \cdot \nabla_\perp B_k^d(\mathbf{x})\,\mathrm{d}\mathbf{x} \tag{66}$$

$$\hat{s}_{\mathrm{i}kj} \stackrel{\mathrm{def}}{=} C_{\mathrm{v}2} \int \frac{\beta_\mathrm{i}}{\tilde{\rho}_\mathrm{i}^2} B_j^d(\mathbf{x}) B_k^d(\mathbf{x})\,\mathrm{d}\mathbf{x} \tag{67}$$

$$\hat{s}_{\mathrm{e}kj} \stackrel{\mathrm{def}}{=} C_{\mathrm{v}2} \int \frac{\beta_\mathrm{e}}{\tilde{\rho}_\mathrm{e}^2} B_j^d(\mathbf{x}) B_k^d(\mathbf{x})\,\mathrm{d}\mathbf{x}. \tag{68}$$

Note that the correct normalization of the skin terms in Ampère's law [4] is of importance. The corresponding normalization constant is

$$C_{\mathrm{v}2}(\kappa_\mathrm{v}) = \mathrm{erf}\left(\frac{\kappa_\mathrm{v}}{\sqrt{2}}\right) - \sqrt{\frac{2}{\pi}}\kappa_\mathrm{v}\left(1 + \frac{\kappa_\mathrm{v}^2}{3}\right)\exp\left(-\frac{\kappa_\mathrm{v}^2}{2}\right) \tag{69}$$

which takes into account the finite extent of the discretized velocity sphere $v_\mathrm{max} = \kappa_\mathrm{v} v_\mathrm{th}$ [see also Eq. (53)]. The discretized current-assignment vector $\mathbf{j}_\mathrm{e}$ of the electrons can be written as

$$j_{\mathrm{e}k} \stackrel{\mathrm{def}}{=} \sum_{p=1}^{N_\mathrm{e}} p_{\|p} w_{\mathrm{e}p} B_k^d(\mathbf{x}_p) \tag{70}$$

and the corresponding gyro-averaged current-assignment vector of the ions is (see Appendix A):

$$\langle j_{\mathrm{i}k}\rangle \stackrel{\mathrm{def}}{=} \frac{1}{\widetilde{N}_{\mathrm{i}p}} \sum_{p=1}^{N_\mathrm{i}} p_{\|p} w_{\mathrm{i}p} \sum_{v=1}^{\widetilde{N}_{\mathrm{i}p}} B_k^d[\mathbf{R}_p + \boldsymbol{\rho}_{\mathrm{i}p}^v]. \tag{71}$$

8.2. Adjusting the control variate by the solution $A_\|$ (scheme one and two)

In Ampère's law the skin terms cancel with the adiabatic current (see Section 3). The control variates method enables us to directly implement the cancellation of terms into the numerical scheme.

We want to show that the two schemes [10,22] presented recently can be derived rigorously with the control variates method. The key idea is to define the control variate as the part responding adiabatically to the magnetic potential $\langle A_\|\rangle_\mathrm{e}$, Eq. (23), in the perturbation of the distribution function of the electrons:

$$\bar{f}_{\mathrm{e}2}(\mathbf{x},\mathbf{v}) \stackrel{\mathrm{def}}{=} -\frac{e n_0(\mathbf{x})}{m_\mathrm{e}} f_{\mathrm{adj}2}(\mathbf{x}) g_2(\Psi,\tilde{v}), \tag{72}$$

where

$$f_{\mathrm{adj}2}(\mathbf{x}) = A_\|(\mathbf{x}) = \sum_{j=1}^{M} c_j B_j^d(\mathbf{x}), \quad g_2(\Psi,\tilde{v}) \stackrel{\mathrm{def}}{=} \frac{p_\| \exp(\tilde{v})}{(2\pi)^{3/2} v_\mathrm{the}^5(\Psi)}. \tag{73}$$

Note that the coefficient vector $\mathbf{c}$ is identical with the coefficient vector in Eq. (65).

The matrix representation of the control variates method [see also Eq. (51)] is given by

$$\mu_0 \tilde{\mathbf{j}}_\mathrm{e} = (\widehat{\mathbf{S}}_\mathrm{e} - \mathbf{S}_\mathrm{e})\mathbf{c} + \mu_0 \mathbf{j}_\mathrm{e}, \tag{74}$$

where the diminishing matrix $\mathbf{S}_\mathrm{e}$ is defined as

$$s_{\mathrm{e}kj} \stackrel{\mathrm{def}}{=} \frac{\mu_0 e^2}{m_\mathrm{e}} \sum_{p=1}^{N_\mathrm{e}} n_0(\mathbf{x}_p) B_j^d(\mathbf{x}_p) B_k^d(\mathbf{x}_p) p_{\|p} g_2(\mathbf{x}_p,\mathbf{v}_p)\Omega_{\mathrm{e}p}. \tag{75}$$

The conventional δf scheme, Eq. (65), can now be replaced by a scheme derived with the control variates method:

$$\widehat{\mathbf{L}} + (\widehat{\mathbf{S}}_\mathrm{i} + \widehat{\mathbf{S}}_\mathrm{e})\mathbf{c} = \mu_0\langle\mathbf{j}_\mathrm{i}\rangle + (\widehat{\mathbf{S}}_\mathrm{e} - \mathbf{S}_\mathrm{e})\mathbf{c} + \mu_0\mathbf{j}_\mathrm{e}. \tag{76}$$

Moving all analytical terms to the left-hand-side and solving for $\mathbf{c}$ we end up with the scheme presented in Ref. [22] herein after referred to as scheme one:

$$\mathbf{c} = (\widehat{\mathbf{L}} + \widehat{\mathbf{S}}_\mathrm{i} + \mathbf{S}_\mathrm{e})^{-1}\mu_0\mathbf{j} \quad \text{where } \mathbf{j} \stackrel{\mathrm{def}}{=} \langle\mathbf{j}_\mathrm{i}\rangle + \mathbf{j}_\mathrm{e}. \tag{77}$$

Usually, in PIC simulations a Fourier filter is imposed onto the coefficient vector $\mathbf{c}$ to filter out the high fluctuating modes to further reduce the noise level (see e.g. Refs. [4,16]). On the one hand, the Fourier filtered coefficient vector

$$\tilde{\mathbf{c}} \stackrel{\mathrm{def}}{=} \mathscr{F}[\mathbf{c}] = \mathscr{F}[(\widehat{\mathbf{L}} + \widehat{\mathbf{S}}_\mathrm{i} + \mathbf{S}_\mathrm{e})^{-1}\mu_0\mathbf{j}] \tag{78}$$

represents the solution of Ampère's law and, on the other hand, determines the spatial part of the new, Fourier filtered, control variate. If this is set in again on the right-hand-side of Eq. (76) we derive,

$$\check{\mathbf{c}} = \mathscr{F}[(\widehat{\mathbf{L}} + \widehat{\mathbf{S}}_\mathrm{i} + \widehat{\mathbf{S}}_\mathrm{e})^{-1}[(\widehat{\mathbf{S}}_\mathrm{e} - \mathbf{S}_\mathrm{e})\tilde{\mathbf{c}} + \mu_0\mathbf{j}], \tag{79}$$

an enhanced form of scheme one with a better convergence rate in respect to the number of markers N_e (see Section 9.2).

It is also possible to derive an iterative version of scheme one by keeping the right-hand-side of Eq. (76) as it is and just solving for the coefficient vector on the left-hand-side

$$\mathbf{c} = (\widehat{\mathbf{L}} + \widehat{\mathbf{S}}_\mathrm{i} + \widehat{\mathbf{S}}_\mathrm{e})^{-1}[(\widehat{\mathbf{S}}_\mathrm{e} - \mathbf{S}_\mathrm{e})\mathbf{c} + \mu_0\mathbf{j}]. \tag{80}$$

We handle this equation as an implicit equation which could not be solved explicitly for $\mathbf{c}$. Hence, we use the iterative method [10] including already a Fourier filter herein after referred to as scheme two:

$$\tilde{\mathbf{c}}^{(n+1)} = \mathscr{F}\{(\widehat{\mathbf{L}} + \widehat{\mathbf{S}}_\mathrm{i} + \widehat{\mathbf{S}}_\mathrm{e})^{-1}[(\widehat{\mathbf{S}}_\mathrm{e} - \mathbf{S}_\mathrm{e})\tilde{\mathbf{c}}^{(n)} + \mu_0\mathbf{j}]\}, \tag{81}$$

where

$$\tilde{\mathbf{c}}^{(0)} = \mathscr{F}[(\widehat{\mathbf{L}} + \widehat{\mathbf{S}}_\mathrm{i} + \widehat{\mathbf{S}}_\mathrm{e})^{-1}\mu_0\mathbf{j}]. \tag{82}$$

Appendix B can be generalized to show that in the absence of a Fourier filter scheme two converges to scheme one under the restriction:

$$\|(\widehat{\mathbf{S}}_\mathrm{e} - \mathbf{S}_\mathrm{e})(\widehat{\mathbf{L}} + \widehat{\mathbf{S}}_\mathrm{i} + \widehat{\mathbf{S}}_\mathrm{e})^{-1}\| < 1. \tag{83}$$

This restriction will be fulfilled for a sufficiently large number of markers N_e as the matrix $\mathbf{S}_\mathrm{e}$ converges to $\widehat{\mathbf{S}}_\mathrm{e}$ for $N_\mathrm{e} \to \infty$.

Scheme two has two advantages compared to scheme one. On the one hand, it is possible to avoid the inversion of the matrix $\widehat{\mathbf{L}} + \widehat{\mathbf{S}}_\mathrm{i} + \mathbf{S}_\mathrm{e}$ which would have to be constructed for each current-assignment procedure. Instead, the matrix $\widehat{\mathbf{L}} + \widehat{\mathbf{S}}_\mathrm{i} + \widehat{\mathbf{S}}_\mathrm{e}$ could be LU decomposed once and reused throughout the whole simulation (see also Appendix B). This is especially useful in situations when the iterative scheme converges already after one or two iterations. On the other hand, the Fourier filter can be easily integrated into the scheme by the Fourier filtered coefficients $\tilde{\mathbf{c}}^{(n)}$ and additionally improves the convergence rate of the iterative scheme significantly. And finally, it gives better results for very small number of markers N_e than the enhanced scheme one, Eq. (79).

8.3. Adjusting the control variate by the current (scheme three and four)

The limitation of scheme one and two is that the choice of the adjusted control variate, Eq. (72), is only able to reproduce part of the electron current density $j_{\|\mathrm{e}}$ analytically namely the adiabatic electron current density $j^{\mathrm{ad}}_{\|\mathrm{e}}$. Hence, we adjust now the control variate in a more systematic approach (see Section 7) to represent the total current density $j_{\|\mathrm{e}}$ of the electrons herein after referred to as scheme three:

$$\bar{f}_{e3}(\mathbf{x},\mathbf{v}) \stackrel{\text{def}}{=} f_{\text{adj3}}(\mathbf{x}) g_2(\Psi,\tilde{v}) \quad \text{and} \quad f_{\text{adj3}}(\mathbf{x}) = -\frac{j_{\parallel e}(\mathbf{x})}{e} = \sum_{j=1}^{M} c_j^{(3)} B_j^d(\mathbf{x}), \tag{84}$$

where the current mass matrix $\widehat{\mathbf{G}}_e$ and the current diminishing matrix $\mathbf{G}_e$ are defined as

$$\hat{g}_{ekj} \stackrel{\text{def}}{=} -e \int_0^{v_{\max}} \left[\int B_j^d(\mathbf{x}) B_k^d(\mathbf{x}) p_{\parallel} g_2(\mathbf{x},\mathbf{v}) \, \mathrm{d}\mathbf{x} \right] \mathrm{d}\mathbf{v} = -eC_{v2} \int B_j^d(\mathbf{x}) B_k^d(\mathbf{x}) \, \mathrm{d}\mathbf{x}, \tag{85}$$

$$g_{ekj} \stackrel{\text{def}}{=} -e \sum_{p=1}^{N_e} B_j^d(\mathbf{x}_p) B_k^d(\mathbf{x}_p) p_{\parallel p} g_2(\mathbf{x}_p,\mathbf{v}_p) \Omega_{ep}. \tag{86}$$

According to Eq. (58) the control variate can be adjusted by

$$\mathbf{c}^{(3)} = \mathbf{G}_e^{-1} \mathbf{j}_e \tag{87}$$

so that the refined current density vector [see also Eq. (59)] is given by

$$\tilde{\mathbf{j}}_e = (\widehat{\mathbf{G}}_e - \mathbf{G}_e)\mathbf{c}^{(3)} + \mathbf{j}_e = \widehat{\mathbf{G}}_e \mathbf{G}_e^{-1} \mathbf{j}_e. \tag{88}$$

Scheme three can be adapted further for a Fourier filtered control variate by

$$\tilde{\mathbf{j}}_e = (\widehat{\mathbf{G}}_e - \mathbf{G}_e)\mathscr{F}(\mathbf{G}_e^{-1}\mathbf{j}_e) + \mathbf{j}_e. \tag{89}$$

Alternatively, it is possible to derive (see Appendix B) an iterative version, Eq. (B.5), of scheme three herein after referred to as scheme four:

$$\tilde{\mathbf{j}}_e \approx \sum_{n=0}^{N_{\text{it}}} \mathbf{j}_e^{(n)} \quad \text{where } \mathbf{j}_e^{(n+1)} = \mathbf{j}_e - \mathbf{G}_e \tilde{\mathbf{c}}^{(n)}, \quad \tilde{\mathbf{c}}^{(n)} = \mathscr{F}\left(\widehat{\mathbf{G}}_e^{-1} \sum_{i=0}^{n} \mathbf{j}_e^{(i)} \right), \tag{90}$$

where $\mathbf{j}_e^{(0)} = \mathbf{j}_e$ and N_{it} the number of iterations. The condition of convergence is

$$\|\mathbf{I} - \mathbf{G}\widehat{\mathbf{G}}^{-1}\| < 1 \tag{91}$$

which is fulfilled for a sufficiently large number of markers N_e as the matrix $\mathbf{G}$ converges to $\widehat{\mathbf{G}}$ for $N_e \to \infty$.

8.4. Adjusting the control variate by a least square fit (scheme five)

Beside the schemes introduced so far it is also possible to discretize Ampère's law with the least square fit scheme derived in Section 7. The matrix $\mathbf{T}_e$, Eq. (62), and the vector $\mathbf{r}_e$, Eq. (63) have to be built up with the electron markers N_e for $g(\mathbf{x}_p,\mathbf{v}_p) = g_2(\mathbf{x}_p,\mathbf{v}_p)$ and $\tau_p = p_{\parallel p}\Omega_p$. Inserting the coefficient vector $\mathbf{c}$, Eq. (61), into Eq. (88) and imposing a Fourier filter we derive the least square fit scheme herein after referred to as scheme five:

$$\mu_0 \tilde{\mathbf{j}}_e = (\widehat{\mathbf{G}}_e - \mathbf{G}_e)\mathscr{F}(\mathbf{T}_e^{-1}\mathbf{r}_e) + \mu_0 \mathbf{j}_e. \tag{92}$$

8.5. Including the control variate in the charge-assignment procedure

The schemes presented so far would not handle the inaccuracy problem in the quasi-neutrality equation properly, Eq. (24). After Ampère's law has been solved with one of the noise reduction schemes one to five, the control variate $\bar{f}_{e2}$, Eq. (72), can be applied to the charge-assignment procedure (see Ref. [10]) of the quasi-neutrality equation:

$$\tilde{\mathbf{b}}_e = (\widehat{\mathbf{U}}_e - \mathbf{U}_e)\tilde{\mathbf{c}} + \mathbf{b}_e = \mathbf{b}_e - \mathbf{U}_e \tilde{\mathbf{c}}, \tag{93}$$

where

$$\hat{u}_{ekj} \stackrel{\text{def}}{=} -\frac{e}{m_e} \int\int n_0(\mathbf{x}) B_j^d(\mathbf{x}) B_k^d(\mathbf{x}) g_2(\mathbf{x},\mathbf{v}) \, \mathrm{d}\mathbf{x} \, \mathrm{d}\mathbf{v} = 0, \tag{94}$$

$$u_{ekj} \stackrel{\text{def}}{=} -\frac{e}{m_e} \sum_{p=1}^{N_e} n_0(\mathbf{x}_p) B_j^d(\mathbf{x}_p) B_k^d(\mathbf{x}_p) g_2(\mathbf{x}_p,\mathbf{v}_p) \Omega_{ep}. \tag{95}$$

We suppose here that $\mathbf{b}_e$ is the electron charge-assignment vector calculated either with the "direct δf" or δf method (see Section 5).

9. Simulations

9.1. Numerical methods

We use the GYGLES code originally written for linear gyrokinetic δf PIC simulations in toroidal geometry [15]. The version used here has been extended to electromagnetic perturbations [see e.g. Eq. (39)] and its numerical methods are described in detail in Ref. [4]. All five schemes derived in Section 8 have been implemented in the GYGLES code which uses a finite element discretization with B-splines for the quasi-neutrality equation, Eq. (15), and Ampère's law, Eq. (16).

9.2. Shear Alfvén waves in the MHD limit $k_\perp \to 0$

9.2.1. The numerical model parameters

Our model problem consists of a damped shear Alfvén wave simulated in a slab with the field equations, Eqs. (15) and (16), where we have excluded the ion sound wave by suppressing the (parallel) motion of the ions, i.e. by setting $\beta_i = 0$ and $\delta f_i = 0$.

The mode wave numbers are $k_x\tilde{\rho}_i = 0.023$, $k_y\tilde{\rho}_i = 0.015$ and $k_z\tilde{\rho}_i = 7.43 \times 10^{-4}$. The box size is given by $L_x/\rho_i = 273$, $L_y/\rho_i = 419$ and $L_z/\rho_i = 8457$ which corresponds to the Wendelstein 7-X stellarator [23] in its cylindrical approximation [4]. The ratio of the ion mass (deuteron) to the electron mass is $m_i/m_e = 3670$. We consider a homogeneous plasma without any gradients and with equal ion and electron temperature $T_i = T_e = 5\,\mathrm{keV}$ and two high beta cases, $\beta_e = 3.04\%$ and $\beta_e = 30.4\%$ corresponding to the number densities of $n_0 = 1.89 \times 10^{20}$ particles/m^3 and $n_0 = 1.89 \times 10^{21}$ particles/m^3 with a magnetic field of $B = 2.5$ T. Four quadratic B-splines in radial (x-)direction are sufficient [4] while a phase factor transformation [15] is used in the parallel (z-)direction on top of four quadratic B-splines. All schemes derived in Section 8 include a Fourier filter in both the x- and z-direction. The loading of the markers in velocity space is uniform in the $(p_\parallel, v_\perp)$-plane and consequently guarantees in contrast to a Maxwellian allocation a good sampling rate at high velocities. The time step has been converged to $\Delta t = 12/\Omega_{ci}$ where $\Omega_{ci} = 120 \times 10^6$ rad/s.

The solution of the dispersion relation for the warm electron response of $\omega_A \ll k_\parallel v_{the}$ becomes for the frequency of the shear Alfvén wave (see Ref. [6]):

$$\omega_A = \pm k_\parallel v_A \sqrt{1 + (k_\perp \tilde{\rho}_i)^2} \quad \text{where } v_A \overset{\text{def}}{=} \frac{B}{\sqrt{\mu_0 m_i n_0}}. \tag{96}$$

For the case of $\beta_e = 3.04\%$ we get $v_A = 2.805 \times 10^6$ m/s and $\omega_A/\Omega_{ci} = 4.2601 \times 10^{-3}$ which is plotted for benchmark purpose as a dashed line in Figs. 2–4(a). The values for the very high beta case, $\beta_e = 30.4\%$, are $v_A = 8.872 \times 10^5$ m/s and $\omega_A/\Omega_{ci} = 1.3472 \times 10^{-3}$ which is plotted as dashed line together with the corresponding simulation results in Fig. 4(b).

9.2.2. The illustrated inaccuracy problem

Our focus is on the simulation in the MHD limit $k_\perp \to 0$ because it is the most challenging test case for the inaccuracy problem as the adiabatic part of the electron response to $\langle A_\parallel \rangle_e$ becomes the dominant part of the perturbation to the distribution function δf_e.

Fig. 1 shows the velocity sphere of the electrons in pitch-angle $\zeta = \arctan(v_\perp/p_\parallel)$ and velocity v normalized to the thermal velocity v_{the}. The absolute value of the sum over the weights $\bar{w}_{ep}$ divided by the Jacobian $J = v$ is plotted as a function of the polar coordinates $(\zeta, v/v_{the})$. In Fig. 1(a), we can see the exposed adiabatic part of δf_e. In Fig. 1(b), the "noise reduced" weights $\hat{w}_{ep}$, Eq. (40), have been plotted. It is impressive to see that the structure of the nonadiabatic part is four orders of magnitude smaller than the adiabatic part. Additionally, the nonadiabatic part is focused around $\zeta = 0$ where the electrons have no $p_\parallel$-component.

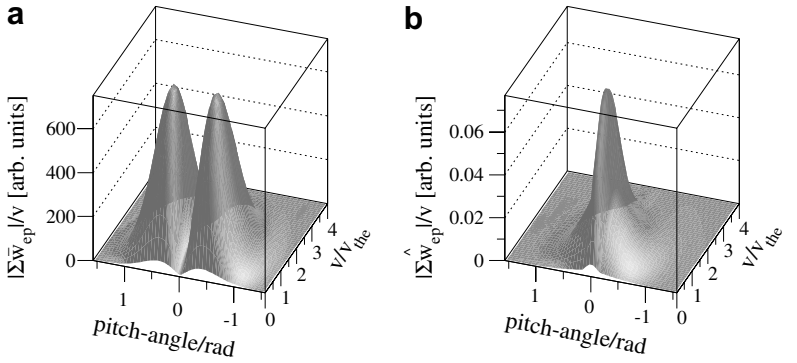

Fig. 1. The perturbed particle number in velocity space as a function of pitch-angle ζ and normalized velocity v/v_{the} for the case of $\beta_e = 3.04\%$. In (a), adiabatic and nonadiabatic electrons, in (b), only the much smaller ($\approx 10^{-4}$) nonadiabatic part of the electrons.

9.2.3. Improvements in respect to the conventional δf scheme

In the following, we will show a convergence study of the oscillation frequency ω_A/Ω_{ci} of the shear Alfvén wave in respect to the number of electron markers N_e for different schemes. By means of Fig. 2 improvements in respect to the conventional δ*f* scheme with a Fourier filtered solution vector [4] are presented for the case of $\beta_e = 3.04\%$.

The conventional δ*f* (filled circles) needs a large velocity sphere of $\kappa_v = 6.75$ and a large number of markers $N_e \approx 10^7$ to converge to the correct result. The usage of the correct normalization of the skin terms, Eq. (69), in Ampère's law (stars), gives already an improvement of one order of magnitude in the number of markers required. This is due to the fact that the velocity sphere could be significantly reduced to $\kappa_v = 4$ (see Ref. [4]). The next reduction of one order of magnitude in N_e is achieved using scheme one (squares) in its rudimentary form, Eq. (77), published in Ref. [22].

However, scheme one is not implemented correctly as long as the control variate is not included in the charge-assignment procedure (triangles), Eq. (93), which leads to a further reduction of one order of magnitude in N_e for converged results. For a slab simulation nearly the same result (down triangles) can be achieved with scheme one in its rudimentary form when the markers are initially distributed symmetrically around the pitch-angle $\zeta = 0$ in velocity sphere. In this case, the numerical evaluation of the integral, Eq. (24), is by construction zero. Unfortunately, for more realistic configurations, the latter method would not be practicable as the marker positions would evolve during the simulation for both velocity spheres, $\pm p_\parallel$, differently.

Finally, a reduction of more than one order of magnitude in N_e can be achieved by a Fourier filtered control variate (open circles) used in scheme two [10].

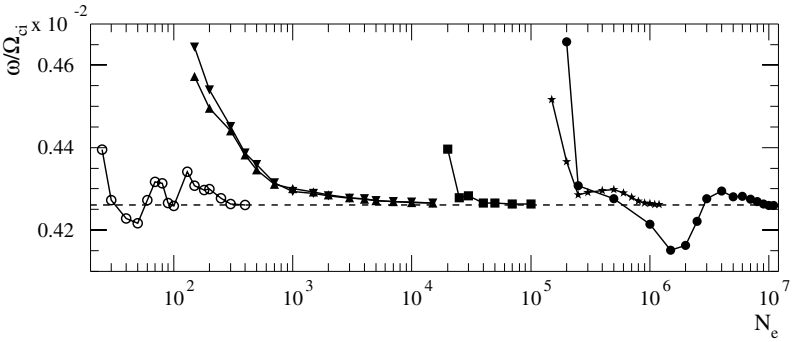

Fig. 2. Convergence study of the frequency ω/Ω_{ci} of the shear Alfvén wave in respect to the number of electron markers N_e for the case of $\beta_e = 3.04\%$. Solutions of the dispersion relation (dashed), conventional δ*f* scheme (filled circles), skin term normalization (stars), scheme one as in Ref. [22] (squares), control variate implemented in charge-assignment (triangles), symmetric distribution of markers in velocity sphere (down triangles) and scheme two (10 iterations) [10] (open circles).

If we sum up all improvements, beginning with the conventional δf scheme and ending at the final form of scheme one, a reduction by more than four orders of magnitude in N_e can be observed for the same quality of results. Thus, the execution time of the simulation can be sped up drastically.

9.2.4. Comparison of the derived schemes

In Fig. 3, the frequency ω_A/Ω_{ci} of the shear Alfvén wave simulation as a function of N_e is shown in (a) as result of scheme one and two and in (b) as result of scheme three and four (see Section 8) for the case of $\beta_e = 3.04\%$. The results of the iterative scheme two and four are presented for different numbers of iterations: one (filled circles), two (stars), three (squares) and ten (triangles). It can be clearly seen that for an increasing number of iterations the convergence property in N_e improves. Already for two iterations only $N_e \approx 1000$ are sufficient for converged results. Thereby the difference between the results of scheme two and four are very small for one and two iterations. Only for higher numbers of iterations and $N_e < 300$ the difference does become apparent. It is also to note that for a large number of iterations scheme two converges to enhanced scheme one, Eq. (79), (open circles) as long as $N_e > 70$ and correspondingly scheme four to scheme three (open circles). For very small numbers of electron markers $N_e < 80$ scheme one and two differ as the implementation of the Fourier filtered control variate differs.

Finally, in Fig. 4(a) and (b), we compare the iterative schemes two (circles) for 10 iterations (converged iterative results) and the direct schemes three (stars) and five (squares) with each other.

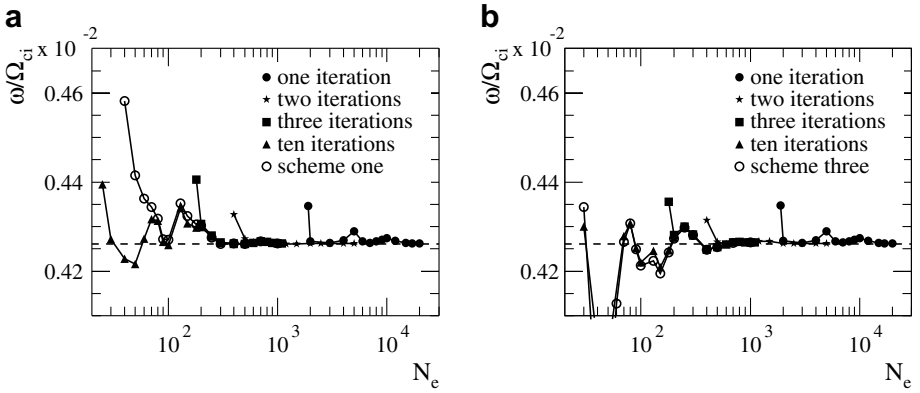

Fig. 3. Convergence study of the frequency ω/Ω_{ci} of the shear Alfvén wave in respect to the number of electron markers N_e for the case of $\beta_e = 3.04\%$. Solution of the dispersion relation (dashed). In (a) scheme one (open circles) and iterative scheme two; in (b) scheme three (open circles) and iterative scheme four. The number of different iterations are: one (filled circles), two (stars), three (squares) and ten (triangles).

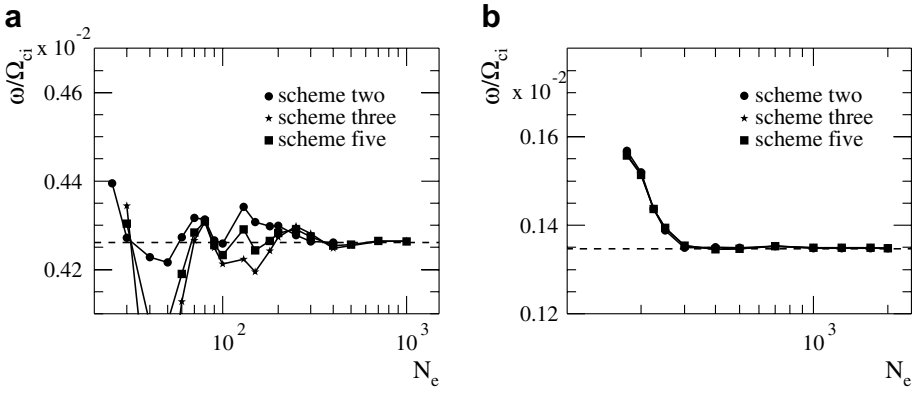

Fig. 4. Convergence study of the frequency ω/Ω_{ci} of the shear Alfvén wave in respect to the number of electron markers N_e for the case of $\beta_e = 3.04\%$ in (a) and $\beta_e = 30.4\%$ in (b). Solutions of the dispersion relation (dashed), scheme two (circles) for 10 iterations, scheme three (stars) and scheme five (squares).

In Fig. 4(a), for the case of $\beta_e = 3.04\%$ all schemes show converged results in the 1% range in respect to the number of electron markers for $N_e \gtrsim 180$. Similar convincing results could be already achieved with the iterative schemes two and four for only three iterations. For $N_e > 70$ the least square fit scheme (five) shows better results than the moment adjusting scheme (three). However, all three schemes give similar results in the MHD limit as the control variates of all three schemes have the same velocity dependence and differ only in their spatial parts.

In Fig. 4(b), for the case of $\beta_e = 30.4\%$ the results of all three schemes are nearly identical. Increasing β_e by an order of magnitude makes the adiabatic part of the distribution function δf_e^{ad} even more dominant over the nonadiabatic part δf_e^{nonad}. In the limiting case of a vanishing nonadiabatic part all three schemes provide identical results. The number of electron markers needed for converged results in the 1% range is $N_e \gtrsim 300$ which is in the same range of markers needed for converged results in Fig. 4(a). Thus, the accuracy of the results is hardly influenced by an increase of β_e by an order of magnitude although the inaccuracy problem becomes much more pronounced. This remarkable property of the new schemes is in strict contrast to the performance of the conventional δf scheme.

10. Conclusions

We have shown that the inaccuracy problem of electromagnetic gyrokinetic PIC simulation, due to the domination of the adiabatic part of the electron response to the magnetic potential $\langle A_\parallel \rangle_e$, can be handled with an adjustable control variates method. Based on this method we have derived five schemes (see Table 1) which can be sub-classified into three direct schemes (one, three and five) and the two iterative counterparts of schemes one and three called scheme two and four. The iterative schemes can be advantageous in respect to computational effort, if a matrix inversion mandatory for each charge-/current-assignment procedure could be handled with an LU decomposition calculated only once at the initialization process of the code.

For the simulation of shear Alfvén waves in a slab at the MHD limit $k_\perp \to 0$ a reduction of more than four orders of magnitude in the number of electron markers N_e can be achieved compared to the conventional δf scheme. The converged results have a relative error of only $\approx 10^{-4}$ in the oscillation frequency ω_A with respect to the analytic solution of the dispersion relation. All five schemes reach converged results in the $<1\%$ range with $\gtrsim 300$ electron markers. The basic convergence property with N_e seems to be nearly unaffected by an increase of β_e by one order of magnitude from $\beta_e = 3.04\%$ to $\beta_e = 30.4\%$. Thus, a significant increase of the inaccuracy problem seems to have very little effect on the accuracy of the derived schemes.

The wave numbers used in our simulations correspond with the $m = 1$ mode in actual plasma devices, e.g. the Wendelstein 7-X stellarator [23]. Accurate computation of low-m modes is necessary for nonlinear simulation of plasma turbulence, where all modes are coupled and self-generated zonal flows have to be treated correctly. Even electromagnetic simulations of modes with moderate $k_\perp$ benefit from the schemes derived here. As the conventional δf method can be used for linear and nonlinear simulations as well as for three-dimensional configurations, all the derived schemes have preserved this vast applicability without any restriction. The required adaptations of an existing δf code are small and only a moderate amount of additional computational time per marker is needed.

The $p_\parallel$-formalism gives the information needed to construct heuristically scheme one and two for the particular case we have considered here. The control variate is tuned especially for this regime. Schemes three, four and five use a control variate with the same velocity dependence as schemes one and two but a more systematically derived adjustable spatial part. These schemes are derived under more general assumptions and would be advantageous for other cases where the adiabatic response to $A_\parallel$ is not the dominate part in the distribution function. However, for the simulation of shear Alfvén waves in the MHD limit all schemes give similar good results.

In general, the control variates method takes advantage of the information about the shape, i.e. the smoothness, of the distribution function $f(\mathbf{x}, \mathbf{v})$ which is usually not considered in the charge-/current-assignment procedure. The control variate could be adapted to include any part of the ion/electron distribution function $f_{i,e}$. The systematic approach in deriving the adjustable control variate (see Section 7) could be extended to velocity space. For example, moments of the distribution functions $f_{i,e}$ could be calculated to

adjust the control variate in velocity space. One of the most general systematic approaches would be a five dimensional B-spline fit function. In such a case, the resolution of the velocity grid could be quite coarse to represent only the coarse structure of the distribution functions $f_{\mathrm{i,e}}$.

The fine structures would be still represented by the weights of the markers which would act as the complement. Such a "two scale" method would have the characteristics of a hybrid method between Semi-Lagrangian (see e.g. Ref. [24]) and PIC method as the main part of the distribution functions would be represented "noise free" on the coarse grid.

Acknowledgments

We acknowledge the support of J. Nührenberg, S. Heinzel and H. Lederer for this work and hold K. Appert in great respect for his knowledge about PIC methods and his hospitality. Especially, we thank S.J. Allfrey, A. Bottino and R. Kleiber for discussions.

Appendix A. Gyro-averaged charge-assignment with the control variates method

Keeping the structure of the discretized control variates method derived in Eq. (51), we can generalize it for a gyro-averaged charge-assignment

$$\langle\tilde{\mathbf{b}}\rangle = (\langle\widehat{\mathbf{A}}\rangle - \langle\mathbf{A}\rangle)\mathbf{c} + \langle\mathbf{b}\rangle, \tag{A.1}$$

where the symbols $\langle\cdot\rangle$ are a way to indicate the now modified vectors and matrices in Appendices A and C.

The gyro-averaged charge-assignment vector $\langle\mathbf{b}\rangle$, originating from Eq. (11), can be discretized in the B-spline basis by

$$\langle b_k\rangle = \frac{1}{2\pi}\sum_{p=1}^{N_s} w_p \oint B_k^d[\mathbf{R}_p + \boldsymbol{\rho}_p(\alpha)]\,\mathrm{d}\alpha. \tag{A.2}$$

The integral over the gyro-phase angle α is usually discretized with an N-point discrete sum (see Refs. [25,16]) of gyro-points distributed equidistantly over the gyro-ring:

$$\frac{1}{2\pi}\oint B_k^d[\mathbf{R}_p + \boldsymbol{\rho}_p(\alpha)]\,\mathrm{d}\alpha \approx \frac{1}{\widetilde{N}_p}\sum_{v=1}^{\widetilde{N}_p} B_k^d[\mathbf{R}_p + \boldsymbol{\rho}_p^v] \tag{A.3}$$

with

$$\boldsymbol{\rho}_p^v \overset{\mathrm{def}}{=} \rho_p[\cos(\alpha_p^v)\mathbf{e}_{\perp 1} + \sin(\alpha_p^v)\mathbf{e}_{\perp 2}], \quad \alpha_p^v \overset{\mathrm{def}}{=} \frac{2\pi v}{\widetilde{N}_p} + \tilde{\alpha}_p, \tag{A.4}$$

where $\mathbf{e}_{\perp 1}$ and $\mathbf{e}_{\perp 2}$ are the unit vectors perpendicular to the magnetic field direction. The gyro-points $\widetilde{N}_p$ are equidistantly distributed over the gyro-ring and rotated for the particle p by a random gyro-phase shift $\tilde{\alpha}_p$. The number of gyro-points $\widetilde{N}_p$ used for the gyro-average of each marker is a linear increasing function of the gyro-radius ρ_p with a minimum of $\widetilde{N}_p = 4$ for $\rho_p \leqslant \tilde{\rho}$ where $\tilde{\rho}$ is the thermal gyro-radius. Inserting Eq. (A.3) into Eq. (A.2) we finally achieve for the gyro-averaged charge-assignment vector

$$\langle b_k\rangle = \frac{1}{\widetilde{N}_p}\sum_{p=1}^{N_s} w_p \sum_{v=1}^{\widetilde{N}_p} B_k^d[\mathbf{R}_p + \boldsymbol{\rho}_p^v]. \tag{A.5}$$

The control variate can be chosen now either as a function of the gyro-center coordinate $\mathbf{R}$ or the coordinate $\mathbf{x}$ of configurational space:

Firstly, we will choose two control variates as function of the gyro-center coordinate $\mathbf{R}$:

(1) The simple choice is to subtract the control variate at the gyro-center position from the gyro-center distribution $f(\mathbf{R},\mathbf{v})$

$$\bar{f}_1(\mathbf{R}, p_\parallel, \tilde{\mu}) \stackrel{\text{def}}{=} g(\mathbf{R}, \mathbf{v}) \sum_{j=1}^{M} c_j^{(1)} B_j^d(\mathbf{R}). \tag{A.6}$$

In this case, one gets for the corresponding matrices:

$$\langle \hat{a}_{1kj} \rangle \stackrel{\text{def}}{=} \frac{1}{2\pi} \int B_j^d(\mathbf{R}) g(\mathbf{R}, \mathbf{v}) B_\parallel^\star \oint B_k^d(\mathbf{x}) \delta(\mathbf{R} + \boldsymbol{\rho}(\alpha) - \mathbf{x}) \, \mathrm{d}\alpha \, \mathrm{d}\mathbf{R} \, \mathrm{d}p_\parallel \, \mathrm{d}\tilde{\mu} \, \mathrm{d}\mathbf{x} \tag{A.7}$$

$$\langle a_{1jk} \rangle \stackrel{\text{def}}{=} \sum_{p=1}^{N_s} B_j^d(\mathbf{R}_p) g(\mathbf{R}_p, \mathbf{v}_p) \Omega_p \frac{1}{\widetilde{N}_p} \sum_{v=1}^{\widetilde{N}_p} B_k^d[\mathbf{R}_p + \boldsymbol{\rho}_p^v]. \tag{A.8}$$

(2) Furthermore, the control variate can be gyro-averaged and subtracted at the gyro-center position from the gyro-center distribution $f(\mathbf{R}, \mathbf{v})$

$$\bar{f}_2(\mathbf{R}, p_\parallel, \tilde{\mu}) \stackrel{\text{def}}{=} g(\mathbf{R}, \mathbf{v}) \sum_{j=1}^{M} c_j^{(2)} \frac{1}{2\pi} \oint B_j^d(\mathbf{R}_p + \boldsymbol{\rho}) \, \mathrm{d}\alpha. \tag{A.9}$$

which would be either useful for $\langle \phi \rangle$ or $\langle A_\parallel \rangle$ as the adjustable part of the control variate (see Section 8.2). The corresponding matrices are

$$\begin{aligned} \langle \hat{a}_{2kj} \rangle \stackrel{\text{def}}{=} & \int g(\mathbf{R}, \mathbf{v}) B_\parallel^\star \frac{1}{2\pi} \oint B_j^d(\mathbf{R}_p + \boldsymbol{\rho}) \, \mathrm{d}\alpha \\ & \frac{1}{2\pi} \oint B_k^d(\mathbf{x}) \delta(\mathbf{R} + \boldsymbol{\rho}(\alpha) - \mathbf{x}) \, \mathrm{d}\alpha \, \mathrm{d}\mathbf{R} \, \mathrm{d}p_\parallel \, \mathrm{d}\tilde{\mu} \, \mathrm{d}\mathbf{x} \end{aligned} \tag{A.10}$$

$$\langle a_{2jk} \rangle \stackrel{\text{def}}{=} \sum_{p=1}^{N_s} g(\mathbf{R}_p, \mathbf{v}_p) \Omega_p \frac{1}{\widetilde{N}_p} \sum_{v=1}^{\widetilde{N}_p} B_j^d[\mathbf{R}_p + \boldsymbol{\rho}_p^v] \frac{1}{\widetilde{N}_p} \sum_{v=1}^{\widetilde{N}_p} B_k^d[\mathbf{R}_p + \boldsymbol{\rho}_p^v]. \tag{A.11}$$

which can be also utilized for a solver of the field equations, Eqs. (9) and (10) (see Ref. [26]).

Secondly, the control variate can be chosen as a function of $\mathbf{R} + \boldsymbol{\rho}$ to subtract it from the gyro-center distribution function on the gyro-ring

$$\bar{f}_3(\mathbf{R} + \boldsymbol{\rho}, p_\parallel, \tilde{\mu}) \stackrel{\text{def}}{=} g(\mathbf{R} + \boldsymbol{\rho}, \mathbf{v}) \sum_{j=1}^{M} c_j^{(3)} B_j^d(\mathbf{R} + \boldsymbol{\rho}). \tag{A.12}$$

In this case, we derive the following matrices:

$$\begin{aligned} \langle \hat{a}_{3kj} \rangle \stackrel{\text{def}}{=} & \frac{1}{2\pi} \int \oint g(\mathbf{R} + \boldsymbol{\rho}, \mathbf{v}) B_j^d(\mathbf{R} + \boldsymbol{\rho}) \\ & B_k^d(\mathbf{x}) \delta(\mathbf{R} + \boldsymbol{\rho}(\alpha) - \mathbf{x}) \, \mathrm{d}\alpha B_\parallel^\star \, \mathrm{d}\mathbf{R} \, \mathrm{d}p_\parallel \, \mathrm{d}\tilde{\mu} \, \mathrm{d}\mathbf{x} \end{aligned} \tag{A.13}$$

$$\langle a_{3jk} \rangle \stackrel{\text{def}}{=} \sum_{p=1}^{N_s} \Omega_p \frac{1}{\widetilde{N}_p} \sum_{v=1}^{\widetilde{N}_p} B_j^d[\mathbf{R}_p + \boldsymbol{\rho}_p^v] B_k^d[\mathbf{R}_p + \boldsymbol{\rho}_p^v] g(\mathbf{R}_p + \boldsymbol{\rho}_p^v, \mathbf{v}_p). \tag{A.14}$$

Note that only the matrices of Eqs. (A.10), (A.11), (A.13) and (A.14) are symmetric.

It is a key issue of the control variates method that the matrices $\langle \widehat{\mathbf{A}}_1 \rangle, \langle \widehat{\mathbf{A}}_2 \rangle$ and $\langle \widehat{\mathbf{A}}_3 \rangle$ defined by Eqs. (A.7), (A.10) and (A.13) are calculated as well as the mass matrix, Eq. (46), analytically or at least with a very high precision. Usually, these matrices have to be built up only once at the initialization process of the simulation so that the computational costs for such an assembly can be quite large without changing the overall performance too much. In such a case, it would be possible e.g. to use a further Monte Carlo integration consisting of a much larger number of Monte Carlo particles than markers in the PIC simulation. In addition, one could benefit from an importance sampling technique which would distribute the Monte Carlo particles proportional to the control variate to further reduce the statistical error in the integration of Eqs. (A.7), (A.10) and (A.13). However, this statistical error has to be much smaller than the statistical noise introduced by the charge-assignment procedure of the PIC method itself.

Appendix B. An iterative control variates method

The moment adjusting scheme derived in Section 7, includes the construction of the mass matrix, Eq. (46), and the diminishing matrix, Eq. (49). The mass matrix is independent of the marker positions and can be calculated at the initialization process of the code. Supposed that the mass matrix is not too large, it would be possible to perform an LU decomposition only once which could be used later for inversion purpose with a forward and back substitution of $O(N^2)$ operations. In contrast to this, the diminishing matrix $\mathbf{A}$ has to be calculated at every charge-assignment procedure as it depends on the marker positions which are functions of time. Its inverse $\mathbf{A}^{-1}$ which would be needed in Eq. (59) would have to be calculated consecutively with $O(N^3)$ operations.

In the following, we will present an iterative control variates method just using the LU decomposition of the mass matrix $\widehat{\mathbf{A}}$. Starting with Eq. (59) we derive

$$\begin{aligned}\tilde{\mathbf{b}} &= \widehat{\mathbf{A}}\mathbf{A}^{-1}\mathbf{b} = (\mathbf{A}\widehat{\mathbf{A}}^{-1})^{-1}\mathbf{b} = [\mathbf{I} - (\mathbf{I} - \mathbf{A}\widehat{\mathbf{A}}^{-1})]^{-1}\mathbf{b}, \\ &= (\mathbf{I} - \mathbf{M})^{-1}\mathbf{b} = \sum_{i=0}^{\infty}\mathbf{M}^i\mathbf{b} = \sum_{i=0}^{\infty}\mathbf{b}^{(i)}\end{aligned} \tag{B.1}$$

where

$$\mathbf{M} \stackrel{\text{def}}{=} \mathbf{I} - \mathbf{A}\widehat{\mathbf{A}}^{-1} \quad \text{and} \quad \mathbf{b}^{(i)} \stackrel{\text{def}}{=} \mathbf{M}^i\mathbf{b}, \quad \mathbf{b}^{(0)} \stackrel{\text{def}}{=} \mathbf{b}. \tag{B.2}$$

We used here the Neumann series which can be useful for the approximate inversion of matrices close to the identity matrix. It has the necessary and sufficient convergence condition that $\mathbf{M}$ has to be a square matrix with norm $\|\mathbf{M}\| < 1$ with the consequence that the eigenvalues of the matrix have to be $|\lambda_\sigma| < 1$. As the number of markers N_s is increased the matrices $\widehat{\mathbf{A}}$ and $\mathbf{A}$ are getting closer to each other and finally they become identical in the limit $N_s \to \infty$. Hence, for a sufficiently large number of markers the convergence condition will be fulfilled.

If we approximate $(\mathbf{I} - \mathbf{M})^{-1}$ with a n-term Neumann series, $n > 1$

$$(\mathbf{I} - \mathbf{M})^{-1}\mathbf{b} \approx \sum_{i=0}^{n-1}\mathbf{M}^i\mathbf{b} = \sum_{i=0}^{n-1}\mathbf{b}^{(i)} \stackrel{\text{def}}{=} \tilde{\mathbf{b}}^{(n-1)} \tag{B.3}$$

the $\tilde{\mathbf{b}}^{(n-1)}$ vector can be interpreted to be assembled by a control variates method. The recursive relation for the construction of the $\mathbf{b}^{(n+1)}$ term is

$$\mathbf{b}^{(n+1)} = \mathbf{M}\mathbf{b}^{(n)} = \mathbf{b}^{(n)} - \mathbf{A}\mathbf{c}^{(n)} \quad \text{where } \mathbf{c}^{(n)} \stackrel{\text{def}}{=} \widehat{\mathbf{A}}^{-1}\mathbf{b}^{(n)}. \tag{B.4}$$

For an efficient algorithmic implementation of Eq. (B.4) we rewrite it in a more convenient form

$$\mathbf{b}^{(n+1)} = \mathbf{b} - \mathbf{A}\hat{\mathbf{c}}^{(n)} \quad \text{where } \hat{\mathbf{c}}^{(n)} \stackrel{\text{def}}{=} \widehat{\mathbf{A}}^{-1}\sum_{i=0}^{n}\mathbf{b}^{(i)}. \tag{B.5}$$

Now only the $\mathbf{b}$ vector and the result of the $(n+1)$-term Neumann series have to be stored. For each iteration step the resulting charge-assignment vector can be written as

$$\tilde{\mathbf{b}}^{(n+1)} = \sum_{i=0}^{n}\mathbf{b}^{(i)} + \mathbf{b}^{(n+1)} = \widehat{\mathbf{A}}\widehat{\mathbf{A}}^{-1}\sum_{i=0}^{n}\mathbf{b}^{(i)} + \mathbf{b} - \mathbf{A}\hat{\mathbf{c}}^{(n)} = (\widehat{\mathbf{A}} - \mathbf{A})\hat{\mathbf{c}}^{(n)} + \mathbf{b}. \tag{B.6}$$

Thus, if one compares Eq. (B.6) with Eq. (59), one can see that for an infinite number of iterations $n = \infty$ the control variate $\hat{\mathbf{c}}^{(\infty)}$ has to converge to the control variate of the moment adjusting scheme:

$$\hat{\mathbf{c}}^{(\infty)} = \widehat{\mathbf{A}}^{-1}\sum_{i=0}^{\infty}\mathbf{b}^{(i)} = \mathbf{A}^{-1}\mathbf{b}. \tag{B.7}$$

If one integrates a Fourier filter into the scheme by imposing it in Eq. (B.5) on $\tilde{c}^{(n)} = \mathscr{F}[\hat{\mathbf{c}}^{(n)}]$ the convergence rate of the iterative scheme can be improved significantly. In practice it has been shown that already after a few iterations the iterative control variates method gives a sufficiently good noise reduction. Hence,

further iterations are not necessary and the computational costs are smaller than with the direct moment adjusting scheme which has to perform an LU decomposition instead. Another advantage of a Fourier filtered control variate is a better convergence rate in respect to the number of markers (see Sections 8 and 9).

Appendix C. Gyro-averaged charge-assignment with adjustable control variates methods

Both adjustable control variate schemes (see Section 7) can be generalized for a gyro-averaged charge-assignment. In the case of the moment adjusting scheme, the control variate is given e.g. by [see Eq. (58)]

$$\mathbf{c} = \langle \mathbf{A} \rangle_3^{-1} \langle \mathbf{b} \rangle. \tag{C.1}$$

The matrix $\langle \mathbf{A} \rangle_3$, Eq. (A.13), is in contrast to the matrix $\langle \mathbf{A} \rangle_1$, Eq. (A.7), symmetric which is an important property as it has to be inverted here. Inserting Eq. (C.1) into Eq. (A.1) one can derive the gyro-averaged moment adjusting scheme in its simple form:

$$\langle \tilde{\mathbf{b}} \rangle = \langle \widehat{\mathbf{A}} \rangle_3 \langle \mathbf{A} \rangle_3^{-1} \langle \mathbf{b} \rangle. \tag{C.2}$$

The control variate for the gyro-averaged least square fit scheme can be derived with a minimization of the squares of the offsets at the position of the gyro-points

$$\chi^2 = \sum_{p=1}^{N_s} \tau_p^2 \frac{1}{\widetilde{N}_p} \sum_{v=1}^{\widetilde{N}_p} \left[f[\mathbf{R}_p + \boldsymbol{\rho}_p^v] - g(\mathbf{R}_p + \boldsymbol{\rho}_p^v, \mathbf{v}_p) \sum_{j=1}^{M} c_j B_j^d [\mathbf{R}_p + \boldsymbol{\rho}_p^v] \right]^2 \to \text{Min} \tag{C.3}$$

which gives the following matrix equation

$$\langle \mathbf{T} \rangle \mathbf{c} = \langle \mathbf{r} \rangle, \tag{C.4}$$

where

$$\langle t_{jk} \rangle \stackrel{\text{def}}{=} \sum_{p=1}^{N_s} \tau_p^2 \frac{1}{\widetilde{N}_p} \sum_{v=1}^{\widetilde{N}_p} B_j^d [\mathbf{R}_p + \boldsymbol{\rho}_p^v] B_k^d [\mathbf{R}_p + \boldsymbol{\rho}_p^v] g^2 (\mathbf{R}_p + \boldsymbol{\rho}_p^v, \mathbf{v}_p) \tag{C.5}$$

$$\langle r_k \rangle \stackrel{\text{def}}{=} \sum_{p=1}^{N_s} \tau_p^2 f_p \frac{1}{\widetilde{N}_p} \sum_{v=1}^{\widetilde{N}_p} B_j^d [\mathbf{R}_p + \boldsymbol{\rho}_p^v] g(\mathbf{R}_p + \boldsymbol{\rho}_p^v, \mathbf{v}_p). \tag{C.6}$$

Inserting again Eq. (C.5) into Eq. (A.1) we finally derive for the least square fit scheme:

$$\langle \tilde{\mathbf{b}} \rangle = (\langle \widehat{\mathbf{A}} \rangle_3 - \langle \mathbf{A} \rangle_3) \langle \mathbf{T} \rangle^{-1} \langle \mathbf{r} \rangle + \langle \mathbf{b} \rangle. \tag{C.7}$$

Note that the coefficient vector $\mathbf{c}$ of the schemes derived in this section can be Fourier filtered again to improve the schemes.

References

[1] A.M. Dimits, W.W. Lee, Partially linearized algorithms in gyrokinetic particle simulation, J. Comp. Phys. 107 (1993) 309.
[2] S.E. Parker, W.W. Lee, A fully nonlinear characteristic method for gyrokinetic simulation, Phys. Fluids B 5 (1993) 77.
[3] A.Y. Aydemir, A unified Monte Carlo interpretation of particle simulations and applications to non-neutral plasmas, Phys. Plasmas 1 (1994) 822.
[4] A. Mishchenko, R. Hatzky, A. Könies, Conventional δf-particle simulations of electromagnetic perturbations with finite elements, Phys. Plasmas 11 (2004) 5480.
[5] I. Manuilskiy, W.W. Lee, The split-weight particle simulation scheme for plasmas, Phys. Plasmas 7 (2000) 1381.
[6] W.W. Lee, J.L.V. Lewandowski, T.S. Hahm, Z. Lin, Shear-Alfvén waves in gyrokinetic plasmas, Phys. Plasmas 8 (2001) 4435.
[7] Y. Chen, S.E. Parker, A delta *f* particle method for gyrokinetic simulations with kinetic electrons and electromagnetic perturbations, J. Comp. Phys. 189 (2003) 463.
[8] T.S. Hahm, W.W. Lee, A. Brizard, Nonlinear gyrokinetic theory for finite-beta plasmas, Phys. Fluids 31 (1988) 1940.
[9] J.V.W. Reynders, Gyrokinetic simulation of finite-beta plasmas on parallel architectures, Ph.D. thesis, Princeton University, 1992.
[10] R. Hatzky, A. Könies, A. Mishchenko, Electromagnetic PIC simulations with a δf method using an enhanced control variates method, in: J.W. Connor, O. Sauter, E. Sindoni (Ed.), Theory of Fusion Plasmas, Proceedings of the Joint Varenna-Lausanne International Workshop, 2004, Società Italiana di Fisica, Bologna, 2004, pp. 13–24.

[11] A. Brizard, Nonlinear gyrokinetic Maxwell-Vlasov equations using magnetic coordinates, J. Plasma Phys. 41 (1989) 541.
[12] K. Höllig, Finite Element Methods with B-Splines, Society for Industrial and Applied Mathematics (SIAM), Philadelphia, 2003.
[13] C.K. Birdsall, A.B. Langdon, Plasma physics via computer simulation, in: E.W. Laing (Ed.), Plasma Physics Series, Institute of Physics Publishing, Bristol, 1995, pp. 220–221.
[14] R.W. Hockney, J.W. Eastwood, Computer Simulation using Particles, Adam Hilger, Bristol, 1989, pp. 149–152.
[15] M. Fivaz, S. Brunner, G. de Ridder, O. Sauter, T.M. Tran, J. Vaclavik, L. Villard, Finite element approach to global gyrokinetic particle-in-cell simulations using magnetic coordinates, Comp. Phys. Commun. 111 (1998) 27.
[16] R. Hatzky, T.M. Tran, A. Könies, R. Kleiber, S.J. Allfrey, Energy conservation in a nonlinear gyrokinetic particle-in-cell code for ion-temperature-gradient-driven (ITG) modes in θ-pinch geometry, Phys. Plasmas 9 (2002) 898.
[17] A. Friedman, J.J. Barnard, D.P. Grote, Techniques for robust nonlinear delta-f simulations of beams, in: Proceedings of the International Computational Accelerator Physics Conference, Monterey, C980914, 1998, pp. 174–178.
[18] S.J. Allfrey, R. Hatzky, A revised delta f algorithm for nonlinear PIC simulation, Comp. Phys. Commun. 154 (2003) 98.
[19] C. DeBoor, A practical guide to splines, Applied Mathematical Sciences, vol. 27, Springer, Berlin, 1978.
[20] G. Jost, T.M. Tran, W.A. Cooper, L. Villard, K. Appert, Global linear gyrokinetic simulations in quasi-symmetric configurations, Phys. Plasmas 8 (2001) 3321.
[21] M. Evans, T. Swartz, in: A.C. Atkinson, D.J. Hand, D.A. Pierce, M.J. Schervish, D.M. Titterington (Eds.), Approximating Integrals via Monte Carlo and Deterministic Methods, Oxford Statistical Science Series, vol. 20, Oxford University Press, Oxford, 2000, pp. 206–209.
[22] A. Mishchenko, A. Könies, R. Hatzky, Gyrokinetic simulations with a particle discretization of the field equations, in: J.W. Connor, O. Sauter, E. Sindoni (Eds.), Theory of Fusion Plasmas, Proceedings of the Joint Varenna-Lausanne International Workshop, 2004, Società Italiana di Fisica, Bologna, 2004, pp. 315–321.
[23] G. Grieger, C.D. Beidler, H. Maassberg, E. Harmeyer, F. Herrnegger, J. Junker, J. Kisslinger, W. Lotz, P. Merkel, J. Nührenberg, F. Rau, J. Sapper, A. Schlüter, F. Sardei, H. Wobig, Physics and engineering studies for Wendelstein 7-X, in: Proceedings of the 13th International Conference on Plasma Physics and Controlled Nuclear Fusion Research, Washington, DC, 1990, (International Atomic Energy Agency, Vienna, 1991), vol. 3, pp. 525–532.
[24] V. Grandgirard, M. Brunetti, P. Bertrand, N. Besse, X. Garbet, P. Ghendrih, G. Manfredi, Y. Sarazin, O. Sauter, E. Sonnendrücker, J. Vaclavik, L. Villard, A drift-kinetic Semi-Lagrangian 4D code for ion turbulence simulation, J. Comp. Phys. 217 (2006) 395.
[25] W.W. Lee, Gyrokinetic simulation particle model, J. Comp. Phys. 72 (1987) 243.
[26] A. Mishchenko, A. Könies, R. Hatzky, Particle simulations with a generalized gyrokinetic solver, Phys. Plasmas 12 (2005). Art. No. 062305.